

\*Manuscript

[Click here to view linked References](#)

## CD44 targeted delivery of siRNA by using HA-decorated nanotechnologies for KRAS silencing in cancer treatment

A Tirella<sup>1,2,\*</sup>, K Kloc-Muniak<sup>3</sup>, L Good<sup>3,4</sup>, J Ridden<sup>3</sup>, M Ashford<sup>5</sup>, S Puri<sup>5</sup>, N Tirelli<sup>1,2,6</sup>

<sup>1</sup> Division of Pharmacy and Optometry, Faculty of Biology, Medicine and Health, University of Manchester, Manchester Academic Health Science Centre, Oxford Road, Manchester, M13 9PL, United Kingdom

<sup>2</sup> NorthWest Centre for Advanced Drug Delivery (NoWCADD), Faculty of Biology, Medicine and Health, University of Manchester, Oxford Road, Manchester, M13 9PT, United Kingdom

<sup>3</sup> Tecrea Ltd. 2 Royal College Street, London, NW1 0NH, UK

<sup>4</sup> Department of Pathology and Population Sciences, Royal Veterinary College, Royal College Street, London, NW1 0TU, UK

<sup>5</sup> Advanced Drug Delivery, Pharmaceutical Sciences, IMED Biotech Unit, AstraZeneca, Cambridge, UK

<sup>6</sup> Laboratory of Polymers and Biomaterials, Fondazione Istituto Italiano di Tecnologia, 16163 Genova, Italy

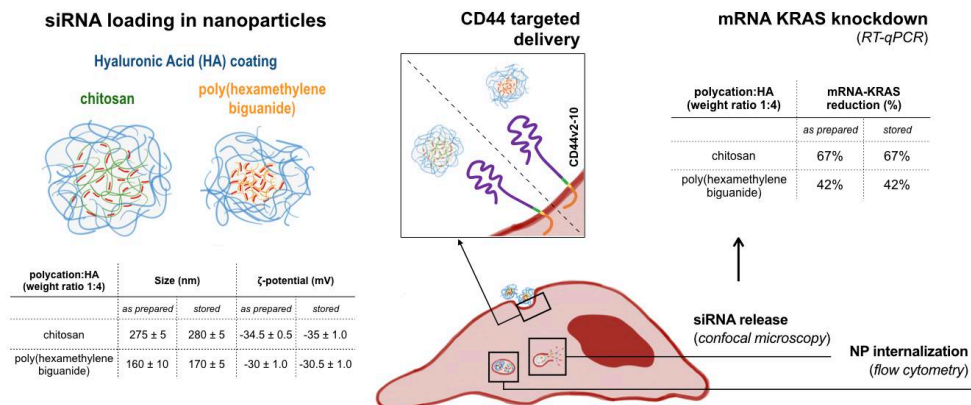
\* Corresponding author: [annalisa.tirella@manchester.ac.uk](mailto:annalisa.tirella@manchester.ac.uk), Division of Pharmacy and Optometry, Stopford Building, FBMH, University of Manchester, Oxford Road, Manchester, M13 9PT, phone +44 (0) 161 275 4769

**Keywords:** Hyaluronan, CD44, polymer therapeutics, siRNA, KRAS

## Abstract

KRAS is a small GTPase that regulates cell proliferation and survival. In tumors, the KRAS gene is mutated, and leading to unregulated tumor growth. Despite the recognized importance of KRAS in cancer, attempts to develop small molecule inhibitors have proved unsuccessful. An alternative strategy is gene silencing and the use of small nucleic acid sequences (e.g. siRNA, shRNA), has been reported to successfully downregulate KRAS. In this study we developed ternary nanocomplexes to deliver an anti-KRAS siRNA to colorectal cancer cells, exploiting the interaction of hyaluronic acid (HA) with CD44 as a means to achieve selective targeting of CD44-positive cancer cells. Two different polycations, poly(hexamethylene biguanide) and chitosan, were complexed with siRNA and coated with HA. Physico-chemical properties and stability of nanoparticles were characterized, including size, surface charge, and degree of siRNA protection. We demonstrate nanoparticle internalization (flow cytometry), siRNA cytosolic release (confocal microscopy) and KRAS silencing (RT-qPCR) in CD44<sup>+</sup>/KRAS<sup>+</sup> colorectal cancer cell line, HCT-116. Further we demonstrate that the uptake of HA-decorated nanoparticles in cancer cells is higher when co-cultured with fibroblasts.

## Graphical abstract



## 1 **1. Introduction**

2 KRAS is a small GTPase involved in the regulation of numerous cellular processes, including  
3 growth, proliferation, survival and other aspects of cellular biology accordingly to its  
4 active/inactive state (Ellis and Clark, 2000). KRAS mutations impair the ability of the KRAS  
5 protein to switch between states, hence mutated KRAS acquires oncogenic properties; such  
6 mutations are observed in approximately 30% of tumors. In particular, pancreatic and  
7 colorectal cancers (Cox et al., 2014; Ross et al., 2017; Stephen et al., 2014), are involved in  
8 tumor initiation and maintenance (Chin et al., 1999; Collins et al., 2012; Zhang et al., 2006)  
9 and are associated with poor prognosis and increased resistance to treatment, including  
10 targeted therapies (e.g. EGFR-TKIs (Überall et al., 2008)). Therefore, it is not surprising that  
11 KRAS is considered an attractive target, but unfortunately an elusive one, since its  
12 intracellular location (Blasco et al., 2011) and very low concentration make its selective  
13 inhibition very challenging. To date, probably the most successful approach has employed  
14 farnesyl transferase inhibitors (KRAS activation requires post-translational farnesylation),  
15 and the use of small molecules to block mutant KRAS and RAS family protein and their  
16 downstream effectors have been developed or are under clinical trial studies (Appels et al.,  
17 2005; Asati et al., 2017; Shin et al., 2018; Wang et al., 2013). Alternatively, small interfering  
18 RNA (siRNA) has been employed to target KRAS (Collisson et al., 2012; Hatzivassiliou et  
19 al., 2013; Kamerkar et al., 2017; Ross et al., 2017), with some systems translated to up to  
20 phase III trials for the intra-tumoral delivery of siRNA to downregulate KRAS, and reduce  
21 KRAS activity in pancreatic tumors (Zorde Khvalevsky et al., 2013).

22 Recently, it has been shown that the regulation of KRAS-mediated signaling in lung  
23 adenocarcinoma is strongly linked to CD44 expression (Zhao et al., 2013): interestingly,  
24 CD44 is both a diagnostic/prognostic marker [16] and a targetable internalization receptor  
25 [15], hence this association may open the way to more selective KRAS-targeted treatments.  
26 In both its standard and higher molecular weight variant isoforms (CD44v2-v10), CD44 has a  
27 major role as a cell surface receptor for hyaluronic acid (HA) (Mattheolabakis et al., 2015;  
28 Ponta et al., 2003) responsible for both its recognition, binding and internalization (Culty et

29 al., 1992). In tumors, CD44 is often expressed as its higher molecular weight variant  
30 isoforms, known to alter cellular behavior and signaling pathways (Culty et al., 1992; Misra  
31 et al., 2008). The variant isoform CD44v6 is of particular interest: it is not only expressed  
32 when tumor associated fibroblasts are activated, but also triggers receptor kinase activities  
33 suggesting again a correlation between CD44 and KRAS in adenocarcinomas (Kim et al.,  
34 1994; Misra et al., 2011). Unsurprisingly, HA has been widely employed in the context of  
35 CD44-targeting therapies, e.g. to improve water solubility or overcome drug resistance  
36 (Auzenne et al., 2007; Coradini et al., 1999; Luo et al., 2002; Yi Luo et al., 2000), with some  
37 successful cases currently in clinical trials (Bassi et al., 2011; Rios de la Rosa et al., 2018).  
38 We are specifically interested in HA-presenting colloidal carriers, which include liposomes  
39 (Surace et al., 2009), solid nanoparticles (Li et al., 2013; Ma et al., 2012; Yu et al., 2013), or  
40 self-assembly nano-systems (Ganesh et al., 2013; Janes et al., 2001; Lallana et al., 2017).  
41 These systems in principle, combine CD44 targeting and CD44-mediated internalization with  
42 the Enhanced Permeation and Retention (EPR) effect (Stylianopoulos and Jain, 2015), which  
43 can further help the selectivity of a targeted therapy.

44 Optimal therapeutic strategies should specifically target the mutated KRAS gene and have  
45 minimal systemic toxicity. To improve the selectivity and delivery of anticancer therapeutics,  
46 an effective strategy may require target-ligand interactions and formulation of nanoparticles  
47 able to promote internalization and cargo release at the desired intracellular site to effectively  
48 address the clinical translation aspects (Birzele et al., 2015; Karousou et al., 2017; Rios de la  
49 Rosa et al., 2017a). One strategy that our group and others have explored over the past decade  
50 is the use of HA-decorated nanoparticles in order to deliver nucleic acid via CD44-HA  
51 interactions. HA provides stability, low protein adsorption and CD44-targeting to the  
52 nanoparticles, which include also a polycation that binds both to HA and the payload  
53 ('glueing' together the carrier) and would then be responsible for endosomal disruption  
54 typically through the 'proton sponge' mechanism (Almalik et al., 2013b; Deng et al., 2014;  
55 Lallana et al., 2017; Parajó et al., 2010). A critical attribute for such systems is indeed the  
56 nature of the polycation, which impacts dramatically on the transfection efficiency. Chitosan;

57 for example, requires a careful optimization of molecular weight and degree of acetylation to  
58 achieve effective siRNA delivery (Lallana et al., 2017). In the context of achieving a CD44-  
59 mediated KRAS silencing therapy, we here investigated the influence of two main descriptors  
60 of the polycation performance, i.e. size and charge density. To enable this, we prepared a  
61 range of nanoparticles employing high molecular weight chitosan and low molecular weight  
62 poly(hexamethylene biguanide), commercially known as Nanocin (Chindera et al., 2016). The  
63 two respectively act as a very large, poorly charged polycation, and as a very small, densely  
64 charged one. Nanoparticles with anti-KRAS siRNA were obtained via combination of  
65 chitosan or Nanocin and HA coating and compared investigating nanoparticles:  
66 stability/efficacy in the presence of RNases and after storage, ability to deliver siRNA in  
67 CD44<sup>+</sup> tumor cells (colorectal cancer cell line HCT-116), and reduction in KRAS expression.  
68 We further investigated the potential of selective delivery of HA-decorated nanoparticles to  
69 cancer cells (HCT-116: CD44<sup>+</sup>, CD44v6<sup>high</sup>) when the latter were co-cultured with CD44<sup>low</sup>  
70 fibroblasts (HDFa).

71

## 72 **2. Materials and Methods**

### 73 **2.1 Nanoparticles and siRNA loading**

74 *2.1.1 Material preparation.* All materials used in this study were handled under RNase free  
75 conditions: solutions were prepared with nuclease-free solvents, and materials were either  
76 purchased RNase free or made RNase free by sequential washing with RNaseZap® RNase  
77 Decontamination Solution (Ambion, LifeTechnologies, UK), 70% v/v EtOH in water, and  
78 finally sterile nuclease-free water (Ambion, Life Technologies, UK) prior to use. Both  
79 polymeric nanotechnologies were manufactured under controlled mixing conditions using  
80 round-bottom vials (2 mL Safe-Lock Tubes, 2 mL, round bottom, PCR clean, Eppendorf,  
81 UK) and magnetic stirring bars (micro 7 mm × 2 mm, Fisher Scientific, UK). Polycations:  
82 Chitosan from crab shells with viscosity average molecular weight of 656 kDa (Almalik et al.,  
83 2013a), was purchased from Sigma Aldrich (Basingstoke, UK; Product code: 51009219,  
84 Lot#WE44069811), and purified prior to use as described elsewhere (Mao et al., 2004).

85 Poly(hexamethylene biguanide), also known as polyhexanide and as Nanocin, with average  
86 molecular weight approximately of 3.2 kDa (www.tecrea.com) was prepared as a sterile  
87 solution with a concentration of 1 mg/mL in RNase free water. Hyaluronic acid (HA) with  
88 weight average molecular weight of 183 kDa (GPC with SLS, viscometer and RI detectors)  
89 was purchased from Contipro (Czech Republic). Selected anti-KRAS sequence (siRNA): 1  
90 mg/mL stock solutions of siRNA were prepared in RNase-free water for both L3-siRNA  
91 (sense 5'-3': GGACUCUGAAGAUGUACCU[dT][dT] 21nt, standard purification, Sigma-  
92 Aldrich, UK) and DY547-labeled L3-siRNA (5'-DY547 GGACUCUGAAGAUGUACCU-  
93 3', Dharmacon, UK). Polymeric solutions used for the manufacturing of nanoparticles were  
94 prepared as follows. Chitosan was dissolved overnight at a concentration of 0.69 mg/mL in  
95 4.6 mM HCl (aq) in nuclease-free water and then pH adjusted to 5 by adding nuclease-free  
96 0.1 M NaOH (aq). Chitosan solution was sterile filtered using 0.45 µm PDVF syringe filters.  
97 Nanocin sterile solution was diluted to 0.69 mg/mL with RNase free sterile water. HA was  
98 dissolved overnight in RNase free water at a concentration of 1.5 mg/mL, and then the pH  
99 was adjusted to 5 by adding nuclease-free 0.1 M HCl (aq). HA solution was sterile filtered  
100 using 0.22 µm PES syringe filters. HA solutions with different concentrations were obtained  
101 by diluting the 1.5 mg/mL solution in nuclease-free water. Sterile siRNA solutions were  
102 prepared at the desired concentration by diluting the 100 µM stock solution (aq) with RNase  
103 free and sterile water and stored at -20°C until use.

104

105 *2.1.2 Preparation of nanoparticles.* HA-coated nanoparticles were prepared with a  
106 concentration of 1 mg/mL in water, using a procedure similar to the one already described by  
107 Lallana et al. (Lallana et al., 2017) for the preparation of RNA-loaded HA/chitosan ternary  
108 complexes. In a typical procedure, a given volume of the 0.69 mg/mL polycation (chitosan or  
109 Nanocin) solution was gently pipetted over the same volume of the siRNA solution (with  
110 concentration adjusted the targeted % wt. loading) under magnetic stirring (1,000 rpm, 25°C).  
111 After 20 min, the polycation/siRNA complex dispersion was gently pipetted to the same  
112 volume of a 1.5 mg/mL HA solution under magnetic stirring (1,000 rpm, 25°C). The final

113 mixture was stirred for further 30 min to obtain siRNA-loaded nanoparticle formulations of  
114 ca. 1 mg/mL (calculated from the nanoparticle polyelectrolyte feed ratio). A typical loading  
115 of 2.3% wt. siRNA (compared to the polycation) was used for nanoparticle characterization  
116 and cell culture experiments. Please note that from now the term nanoparticles (NP) refers to  
117 both HA-coated Nanocin or chitosan nanoparticles.

118

119 *2.1.3 Preparation of nanoparticles varying polycation:HA ratio.* NP were prepared varying  
120 polycation:HA ratio to identify the optimal formulation in terms of size and  $\zeta$  potential. NP  
121 were prepared using HA solutions with the following concentration (polycation:HA ratio):  
122 0.375 mg/mL (1:1), 0.75 mg/mL (1:2), 1.125 mg/mL (1:3) and 1.5 mg/mL (1:4). For  
123 uncoated NP (1:0 ratio), RNase free water (pH adjusted to 5) was used. NP were prepared  
124 using the same procedure described above (Section 2.1.2). Briefly, the polycation/siRNA  
125 complex dispersion was pipetted in an equivalent volume of HA at different concentrations to  
126 vary the polycation:HA weight ratio. Note that in this case the final concentration of NP  
127 varies from 0.35 mg/mL (1:0) to 1 mg/mL (1:4).

128

129 *2.1.4 Preparation of nanoparticles varying siRNA loading.* NP were prepared by loading  
130 different amount of siRNA, i.e. 2.3% wt., 25% wt. weight ratio compared to polycation  
131 content. siRNA solutions were prepared in RNase free and sterile water at different  
132 concentrations, 0.016 mg/mL (2.3% wt.) and 0.172 mg/mL (25% wt.). NP were prepared as  
133 described above (Section 2.1.2).

## 134 **2.2 Nanoparticle characterization**

135 *2.2.1 Dynamic Light Scattering (DLS).* NP (1mg/mL in water) hydrodynamic diameter (Z-  
136 average size), size polydispersity (PDI), and  $\zeta$  potential were measured at 25°C (pre-  
137 equilibration for 2 min; 1 mg/mL) using a Zetasizer Nano ZS (model ZEN3600, Malvern  
138 Instruments Ltd., UK) equipped with a solid state HeNe laser ( $\lambda = 633$  nm) at a scattering

139 angle of 173°. Size distributions were calculated by applying the general-purpose algorithm  
140 and are presented as the average of the Z-average values of three independent samples.

141

142 *2.2.2 Payload protection against RNase.* NP (1mg/mL in water) used in this study were  
143 prepared by loading an amount of siRNA corresponding to 25%wt. of the polycation (13 µM  
144 siRNA solution) +/- HA coating. Briefly, 50 µL of NP were incubated with 50 µL of a  
145 solution of RNase I (AM2294, Ambion, Thermofisher Scientific) (15 mM Tris buffer, 0.3 M  
146 NaCl, pH 7.0) at a concentration of 0, 0.33, and 3.33 U (corresponding to 0, 0.1, 1 and 10 U  
147 of RNase I/mL, respectively). Samples were incubated at 37°C for 30 min. The nuclease  
148 reaction was then quenched with the addition of 7.6 µL of 1.0% SDS (aq). Afterward, 3 µL of  
149 chitosanase (0.066 U/µL, 50 mM acetate buffer, pH 5.0) was added to the mixture, and the  
150 enzymatic reaction was allowed to occur for 3 h at 37°C. Finally, 4.7 µL of a solution of  
151 heparin (80 mg/mL in RNase-free water; corresponding approximately to a negative/positive  
152 charge molar ratio of of 250) was added. The resulting mixture was incubated overnight at  
153 25°C. After centrifugation (13,000 rpm, 30 min), the nucleic acid released in solution was  
154 quantified using polyacrylamide gel electrophoresis (siRNA; 18-well/30 µL, 15% Criterion  
155 TBE-Urea Gel, Biorad; 70 min, 120 V). Gels were finally incubated for 30 min in a 1X  
156 GelRed™ solution and imaged using a UV trans-illuminator (Biorad).

157

158 *2.2.3 Nanoparticle stability.* NP were stored at 4°C for one week and then tested to check  
159 variations in size, surface charge and efficacy (for silencing experiments details refer to  
160 section 2.7).

## 161 **2.3 Cell culture and CD44 characterization**

162 *2.3.1 General cell culture.* All cell culture experiments and following procedures were  
163 performed at the University of Manchester (UK), unless otherwise specified. The human  
164 colorectal carcinoma cell line HCT-116 (CCL-247) was purchased from ATCC (Manassas,  
165 VA, USA) and the adult human dermal fibroblast (HDFa, #C0135C) cell line was purchased



166 from Thermo-Fisher Scientific (UK). Cells were cultured in a humidified 5% (v/v) CO<sub>2</sub> air  
167 atmosphere at 37°C in complete medium, cell culture growth media were supplemented with  
168 10% (v/v) fetal bovine serum (FBS, F7524), 2 mM L-glutamine (G7513) and 1% (v/v)  
169 penicillin–streptomycin (P4333). McCoy’s 5A medium (M8403) and DMEM (D5671) were  
170 used for HCT-116 and HDFa, respectively. Please note that cells were regularly tested for  
171 mycoplasma and used at passage numbers below 20, and that all cell culture products were  
172 purchased from Sigma- Aldrich (Gillingham, UK).

173

174 *2.3.2 CD44 expression: flow cytometry.* Cells were grown in T-75 flasks until reaching ~70%  
175 confluency and harvested using pre-warmed Enzyme-Free, Phosphate Buffer solution (PBS)-  
176 based Cell Dissociation Buffer (#13151-014, Gibco®/Invitrogen, UK). Individual cell  
177 samples were prepared in 1.5 mL Eppendorf tubes by suspending approximately 100,000  
178 viable cells in 100 µL Fluorescence-Activated Cell Sorting (FACS) buffer (PBS, 5% (v/v)  
179 FBS, 0.1% (m/v) NaN<sub>3</sub>) and stained for 30 min at room temperature with the primary  
180 antibody mouse anti-human CD44 (1:100) (156-3C11, Cell Signalling Technology, UK) or  
181 IgG1/IgG2 control (1:10) (AbD Serotec, UK). Excess primary antibody was removed by  
182 centrifugation and cells were incubated for further 30 min at room temperature with the  
183 secondary antibody: goat anti-mouse IgG H&L, AlexaFluor®647-conjugated (1:2000)  
184 (ab150115, Abcam, UK). The expression of total CD44 (CD44pan) was recorded for 10,000  
185 live, individual cells using a BD LSRFortessa cytometer (BD Bioscience, San Jose CA, USA)  
186 equipped with the FACSDiva software (v8.0.1). Data were analyzed with FlowJo (vX.0.7,  
187 Tree Star, Ashland, OR, USA) after gating live cells in the FSC/SSC window and cell singlets  
188 in the FSC-H/FSC-A window, respectively. The median fluorescence intensity (MFI) of the  
189 isotype control for each cell line was used to calculate the MFI fold change for each marker.

190

191 *2.3.3 CD44 expression: immunofluorescence staining.* HCT-116 cells were plated in Ibidi µ-  
192 slide (prod.no. 80826, Ibidi®, Germany) at 70% of confluency (approx. 8,000 cells, 37°C, 5%  
193 CO<sub>2</sub>) and left adhere overnight. Live cells were then stained with the following primary

194 antibodies: i) mouse anti-human CD44 (1:100) (156-3C11, Cell Signaling Technology, UK),  
195 ii) mouse anti-human CD44v3 (1:20) (Clone #3G5, R&D Systems, UK), iii) mouse anti-  
196 human CD44v6 (1:20) (Clone #2F10, R&D Systems, UK); hence detecting only membrane  
197 bound CD44. Briefly, cells were washed with PBS, incubated with mouse anti-human CD44  
198 primary antibody solutions diluted in 1% (w/v) BSA/PBS on ice for 30 min, gently washed  
199 with PBS, and incubated with 1:250 goat anti-mouse IgG H&L, AlexaFluor®488-conjugated  
200 (ab150117, Abcam, UK) on ice for additional 30 min. Cells were finally washed with PBS  
201 (twice), fixed with 4% PFA solution (5 min, RT), washed with PBS and stored in 1 mg/mL  
202 ascorbic acid solution in PBS at 4°C in the dark until further use.

## 203 **2.4 Nanoparticle internalization**

204 NP (0.125 mg/mL, final concentration) for cell experiments were prepared in complete cell  
205 growth medium as follows, a final siRNA concentration of 40 nM (0.5 µg/mL) was obtained.  
206 HA-coated chitosan NP (1 mg/mL in water) were diluted after preparation to a concentration  
207 of 250 µg/mL with sterile and nuclease-free water. The final concentration of 125 µg/mL  
208 used for cell culture experiment was obtained by addition of an equal volume of two-fold cell  
209 culture medium (refer to Supporting Information SI.1 for the preparation of concentrated cell  
210 culture medium). Nanocin/HA NP (1 mg/mL) were diluted after preparation by adding 11.6  
211 µL of nanoparticles to complete cell culture media to a final volume of 1 mL. Note that  
212 kinetic of internalization studies were performed loading DY547-siRNA (L3 sequence: 5'-  
213 DY547 GGACUCUGAAGAUGUACCU-3'; Dharmacon, UK) in NP (i.e. DY547-NP).

214

215 *2.4.1 Quantification of nanoparticle internalization: flow cytometry.* Cells were plated in  
216 Costar tissue culture polystyrene (TCP) 12-well plates with flat bottom (#3513, Corning, UK)  
217 and incubated (37°C, 5% CO<sub>2</sub>) with 125 µg/mL DY547-NP for specific time points: 4, 12,  
218 and 24 h. Untreated cells were used as a negative control. After each incubation time,  
219 nanoparticle-containing medium was removed, cells were washed with PBS (n=3) and  
220 detached using Trypsin-EDTA solution (#59417C, Sigma-Aldrich, UK) for 10 min at room

221 temperature. Trypsin was used to remove any residual membrane-bound nanoparticle,  
222 enabling the detection of internalized nanoparticles exclusively (Rios de la Rosa et al.,  
223 2017b). Cells were pelleted (1000 rpm, 5 min, 25°C) and re-suspended in 400 µL PBS. The  
224 internalization of DY547-NP was determined on 10,000 individual and live cells with the BD  
225 LSRFortessa cytometer (BD Bioscience, San Jose CA, USA) equipped with the FACSDiva  
226 software (v8.0.1). Data were analyzed with FlowJo (vX.0.7, Tree Star, Ashland, OR, USA)  
227 after gating single and live events in the FSC-A/FSC-H and FSC/SSC windows, respectively.  
228 Untreated cells were used as autofluorescence control in order to calculate the median  
229 fluorescence intensity (MFI) fold change over time, as well as the percentage of positive  
230 events for each cell line.

231

232 *2.4.2 Nanoparticle late endosome/lysosome escape: confocal microscopy.* HCT-116 cells  
233 were plated in Ibidi µ-slide (prod.no. 80826, Ibidi®, Germany) at 70% of confluency and left  
234 adhere overnight (37°C, 5% CO<sub>2</sub>). A volume of 100 µL of DY547-NP (125 µg/mL in  
235 complete cell culture media) was added to each well and cells were incubated for 1 h (37°C,  
236 5% CO<sub>2</sub>), DY547-NP containing medium was then removed, cells were gently washed with  
237 PBS (n=2) and co-incubated with 100 nM LysoTracker Green (L7526, Invitrogen, Thermo  
238 Fisher, UK) and 1 µM Hoechst (33342, Invitrogen, Thermo Fisher, UK) solution (37°C, 5%  
239 CO<sub>2</sub>, 10 min). Cells were finally gently washed with PBS (n=2), kept in 1 mg/mL ascorbic  
240 acid solution in PBS and immediately imaged with laser scanning confocal microscope.

241

242 *2.4.3 Nanoparticle uptake and role of HA-coating: confocal microscopy.* HCT-116 cells were  
243 plated in Ibidi µ-slide (prod.no. 80826, Ibidi®, Germany) at 70% of confluency and left  
244 adhere overnight (37°C, 5% CO<sub>2</sub>). HA-coated and uncoated DY547-NP (125 µg/mL in  
245 complete cell culture media) were used. A volume of 100 µL of DY547-NP was added to  
246 each well and cells were incubated for 24 h (37°C, 5% CO<sub>2</sub>), nanoparticle-containing medium  
247 was then removed, cells were gently washed with PBS (n=2), incubated (37°C, 5% CO<sub>2</sub>, 10  
248 min) with 1 µM Hoechst solution in PBS (33342, Invitrogen, Thermo Fisher, UK), cells were

249 gently washed with PBS (n=2), kept in 1 mg/mL ascorbic acid solution in PBS and  
250 immediately imaged with laser scanning confocal microscope.

## 251 **2.5 Co-culture experiments: HCT-116 and fibroblasts**

252 Co-culture experiments were performed using TCP 6-well plates with flat bottom (Prod. No.  
253 3513, Corning, UK). HCT-116 cells were seeded at a density of 10,000 cells/cm<sup>2</sup> on the  
254 bottom of the wells, whereas fibroblasts (HDFa) were seeded on transwell inserts (MW6  
255 Transwell Inserts, 0.4µm PET Membrane, Corning, UK) at a density of 10,000 cells/cm<sup>2</sup>.  
256 Cells were left adhere for 12 h in separate multi-well plates (37°C, 5% CO<sub>2</sub>), then inserts  
257 culturing HDFa cells were transferred to the 6-well plates culturing cancer cells and 3 mL of  
258 complete DMEM was added in each well to allow media exchange between the two  
259 compartments (overnight, 37°C, 5% CO<sub>2</sub>). Cells were co-cultured up to 48 hours (37°C, 5%  
260 CO<sub>2</sub>).

261

262 *2.5.1 Nanoparticle kinetics of internalization in co-culture: flow cytometry.* Cells were  
263 incubated with DY547-NP (125 µg/mL in complete cell culture media) corresponding to a  
264 final 40 nM siRNA concentration, up to 48 hours (37°C, 5% CO<sub>2</sub>). After each time point (4,  
265 12, 24 and 48 h), NP containing medium was removed, cells were washed with PBS (n=3)  
266 and detached using Trypsin-EDTA solution (#59417C, Sigma-Aldrich, UK) for 10 min at  
267 room temperature. Note that trypsin was used to remove any residual membrane-bound  
268 nanoparticle, enabling the detection of internalized DY547-NP only. Cells were pelleted  
269 (1000 rpm, 5 min, 25°C) and re-suspended in 400 µL PBS. The internalization of DY547-NP  
270 was determined on 10,000 individual and live cells with the BD LSRFortessa cytometer (BD  
271 Bioscience, San Jose CA, USA) equipped with the FACSDiva software (v8.0.1). Data were  
272 analyzed with FlowJo (vX.0.7, Tree Star, Ashland, OR, USA) after gating single and live  
273 events in the FSC-A/FSC-H and FSC/SSC windows, respectively. Untreated cells were used  
274 as autofluorescence control in order to calculate the median fluorescence intensity (MFI) fold

275 change over time, as well as the percentage of positive events for each cell line. Untreated  
276 cells were also used as a control.

## 277 **2.6 Imaging: CD44, nanoparticle internalization and siRNA localization**

278 *2.6.1 CD44 expression: inverted microscope.* Images of IF samples were acquired using an  
279 inverted microscope (Leica DMI6000B, Leica Microsystems, UK) coupled with a 5.5 Neo  
280 sCMOS camera (Andor, UK) and the EL6000 fluorescent lamp (Leica Microsystem, UK), all  
281 controlled by *μManager* software (v.1.46, Vale Lab, UCSF, USA). For acquisitions,  
282 immersion oil 63X/1.40-0.60 HC PL Apo objective was used, using I3 filter cube (Leica  
283 Microsystem, UK). Images were post-processed using ImageJ adjusting brightness/contrast  
284 for a better visualization of CD44 (v1.51h, <http://imagej.nih.gov/ij>).

285

286 *2.6.2 Nanoparticle internalization: confocal microscope.* An inverted SP5 laser scanning  
287 confocal microscope (Leica TSC SP5 AOBS, Leica Microsystem, UK) was used to acquire  
288 volumetric datasets of IF stained cells. Acquisitions were performed using the immersion oil  
289 63X/1.40 HCX PL Apo objective. Images were acquired with sequential scan using 405, 488,  
290 546 and 594 nm laser lines. Images were acquired with different settings accordingly to each  
291 experiment, in particular pinhole was kept to 1 airy unit aperture, pixel size adjusted to 150-  
292 165 nm, laser lines settings were adjusted to the dyes, frequency scan and averaged line were  
293 modified accordingly to the sample, whether live or fixed. Images were post-processed using  
294 ImageJ adjusting brightness/contrast for a better visualization of components (v1.51h,  
295 <http://imagej.nih.gov/ij>). Large field images were also used to quantify the amount of siRNA  
296 internalized: briefly, the maximum projection of the siRNA channel was obtained, Otsu  
297 threshold was applied, the area of the signal was measured and expressed as % with respect to  
298 the scanned area.

## 299 **2.7 siRNA delivery and KRAS silencing**

300 NP (0.125 mg/mL, final concentration in complete cell culture media) were used for KRAS  
301 silencing experiments. NP were prepared loading 40 nM (corresponding to 0.5 μg/mL) of L3-

302 siRNA sequence (sense 5'-3': GGACUCUGAAGAUGUACCU[dT][dT] 21nt, standard  
303 purification, Sigma-Aldrich, UK). Refer to the Supplementary Information for detailed  
304 description of siRNA sequences tested for KRAS silencing (Section SI.2). Briefly, HCT-116  
305 cells were seeded at a density of 10,000 cells/cm<sup>2</sup> in TCP 12-well plates with flat bottom  
306 (Thermo Scientific, NUNC MULTIDISH 12, #150628) and left adhere overnight. Cells were  
307 then incubated in complete media containing NP (HA-coated) for 48 hours in a humidified  
308 5% (v/v) CO<sub>2</sub> air atmosphere at 37°C. In the case of Nanocin NP, the media was changed  
309 after 24 hours, which has been found to improve the silencing efficiencies. Nanocin is  
310 compatible with repeat transfection due to relatively low cell toxicity. Lipofectamine™ 2000  
311 was used as control. NP containing media were removed and cells thorough rinsed with PBS  
312 (n=3). The total RNA was extracted using phenol-chloroform method with: TRI Reagent  
313 (Cat. No.: T9424, Sigma-Aldrich). Reverse Transcription Reaction was performed using kit:  
314 High Capacity RNA-to-cDNA kit, Applied Biosystems and finally amplification (qPCR) was  
315 performed using kit: 2xqPCRBIO SyGreen Mix Lo-ROX (Cat.No. PB20.11-05, Applied  
316 Biosystems, UK) following manufacturer's instructions.

### 317 **2.8 Statistical Analysis**

318 Differences between groups were considered to be significant at a P value of <0.05. Statistical  
319 analyses (One-way ANOVA) were performed with GraphPad Prism 7.0 (GraphPad Software,  
320 Inc., San Diego, CA).

321 **3. Results and Discussion**

322 **3.1 Nanoparticles characterization**

323 *3.1.1 Nanoparticle physical stability.* As prepared, all NP showed a rather comparable  
 324 hydrodynamic size, although typically lower for Nanocin (Table 1, Figure 1a and 1b). This is  
 325 likely due to the higher charge density of this polymer, which allows a higher ionic cross-link  
 326 density and therefore also a lower water content in the particles. As expected, the  $\zeta$ -potential  
 327 (surface charge) depended on the polycation:HA weight ratio, and shifted from positive to  
 328 negative values with increasing HA content. With both polycations, a ‘charge inversion’  
 329 occurred at a polycation:HA weight ratio between 1:1 and 1:2; these samples also exhibited  
 330 the largest sizes. At stoichiometry ratios close to the effective complexation between positive  
 331 and negative charges, polyelectrolyte complexes form and keep aggregating due to the  
 332 reduced repulsion, until a size is reached. At this equilibrium, a small imbalance in either of  
 333 the charged components leads to a sufficient surface coverage to grant electrostatic  
 334 stabilization. In deionized water, chitosan-based NP showed a mild agglomeration upon  
 335 storage (size variation less than 5%), independent of the amount of HA. On the contrary,  
 336 Nanocin stability depended on HA: Better stability at high HA content which decreased at  
 337 low (polycation:HA < 1:2), and showed significant increases in size and  $\zeta$ -potential post  
 338 storage. This effect is probably due to the strong interactions between the high-cationic  
 339 density, small-size Nanocin and HA, which significantly reduce the electrostatic stabilization  
 340 due to excess (uncomplexed) negative charges of HA. Due to their better stability, all further  
 341 experiments were conducted with a 1:4 polycation/HA ratio.

**Table 1.** Effect of storage in water on the size and charge of nanoparticles with variable polycation:HA weight ratio.

Polycation:HA <sup>a</sup> (weight ratio)		Size (nm) <sup>b</sup>		$\zeta$ -potential (mV) <sup>b</sup>	
		As prepared	Stored <sup>c</sup>	As prepared	Stored <sup>c</sup>
1:0	<i>chitosan</i>	210 ± 5	210 ± 5	52.0 ± 1.5	52.0 ± 1.0
	<i>Nanocin</i>	120 ± 10	390 ± 100	15.5 ± 7.5	24.0 ± 0.5
1:1	<i>chitosan</i>	270 ± 10	300 ± 15	35.0 ± 1.0	35.0 ± 1.0
	<i>Nanocin</i>	170 ± 10	400 ± 10	21.0 ± 1.0	23.0 ± 1.0
1:2	<i>chitosan</i>	220 ± 5	205 ± 5	-25.5 ± 0.5	-24.5 ± 1.0
	<i>Nanocin</i>	210 ± 75	320 ± 10	-19.0 ± 1.5	-21.0 ± 0.5

1:3	<i>chitosan</i>	230 ± 5	255 ± 15	-31.0 ± 1.0	-32.5 ± 1.0
	<i>Nanocin</i>	180 ± 20	185 ± 5	-30.0 ± 0.5	-31.5 ± 0.5
1:4	<i>chitosan</i>	275 ± 5	280 ± 5	-34.5 ± 0.5	-35.0 ± 1.0
	<i>Nanocin</i>	160 ± 10	170 ± 5	-30.0 ± 1.0	-30.5 ± 1.0

<sup>a</sup> Please note that siRNA was always used at a ratio 2.3%wt. in respect to the polycation weight, hence nanoparticles were prepared also in the absence of HA.

<sup>b</sup> Concentration: 1 mg/mL in deionized water

<sup>c</sup> Storage: 1 week, 4°C in deionized water.

342 *3.1.2 Protection of siRNA against RNase.* We have assessed the stability of siRNA in  
343 nanoparticles (siRNA:polycation 1:4 weight ratio), when they were exposed to different  
344 concentrations of RNase I (Figure 1e). siRNA in solution was already partially degraded at  
345 0.01 U/μL RNase (~10% degradation), with >50% degradation at 0.1 U/μL RNase, whereas  
346 siRNA liberated from nanoparticles was intact even after exposure to 1 U/μL RNase, with no  
347 statistically relevant difference with the two polycations and with/out HA.

348



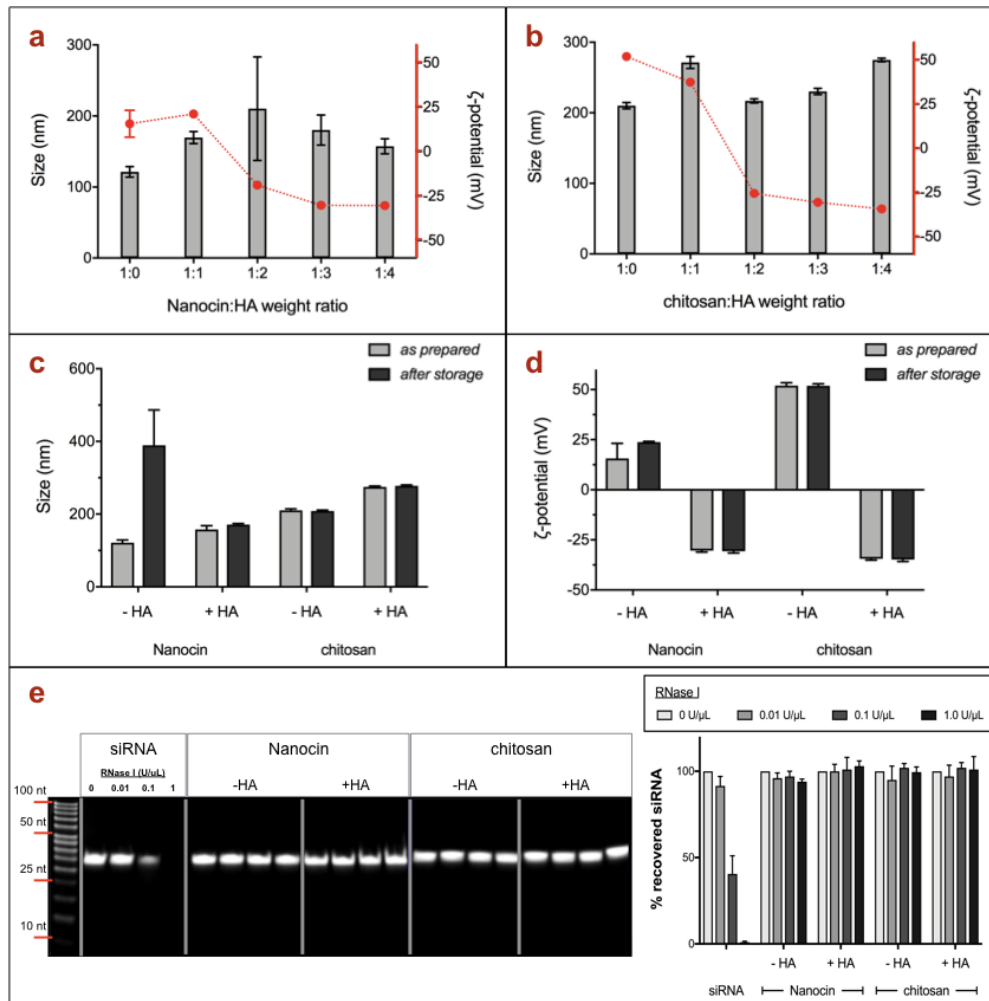


**Figure 1.** Physico-chemical characterization of nanoparticles. Z-average size (histogram) and  $\zeta$ -potential (red dots) of as-prepared Nanocin- (a) and chitosan-based (b) nanoparticles. The effect of storage is respectively shown in (c) and (d) for particles without HA and a 1:4 polycation:HA ratio. A typical PAGE gel analysis (e) shows payload protection for 25% wt. siRNA-loaded nanoparticles after incubation with different concentrations of RNase I (for each column, from left to right: 0, 0.01, 0.1, 1 U/ $\mu$ L). Recovered siRNA is expressed as percentage with respect to its control, each value is reported as average  $\pm$  st.dev. of at least three independent samples.

### 349 3.2 Targeting and internalization of HA-coated nanoparticles

350 3.2.1 CD44 expression. Colorectal cancers have a high incidence of mutation of KRAS, and

351 we have therefore chosen a model of human colorectal cancer, HCT-116 cells, known to

352 present KRAS<sup>G13D</sup> mutation (Alves et al., 2015). HCT-116 also have high CD44 expression

353 (Rios de la Rosa et al., 2017b), and unsurprisingly this is higher than in the cells (HDFa)

354 which we used as a model for stromal component of the tumor microenvironment (Figure 2a).

355 Importantly, HCT-116 cells were positive to CD44 variants commonly associated to

356 malignancies, such as CD44v3<sup>high</sup> (Figure 2c) and CD44v6<sup>high</sup> (Figure 2e), but not CD44v4  
 357 (Figure 2d). No CD44 variants were detected in HDFa (data not shown).

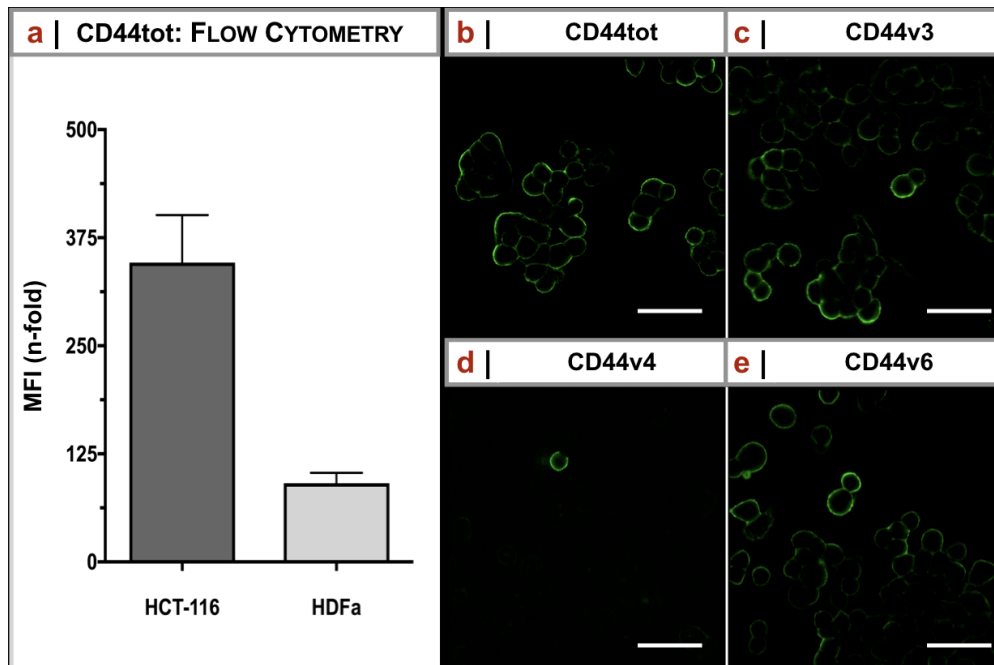


**Figure 2.** Characterization of CD44 expression in the selected cellular models. a) Flow cytometry measurements of total CD44 (all isoforms combined) in HCT-116 and HDFa. Results are expressed as mean  $\pm$  st.dev. ( $n=3$ ,  $N=2$ ). Immunofluorescence (IF) cancer cells (HCT-116) stained for: b) total CD44, c) CD44v3, c) CD44v4 and e) CD44v6. Scale bars 50  $\mu$ m.

358 3.2.2 Nanoparticle internalization: mono-culture vs. co-culture. We have followed the  
 359 kinetics of both NP internalization via flow cytometry using a fluorescently labelled siRNA  
 360 (L3-DY547-NP) for 24 h. NP internalization was firstly investigated on cancer cells and  
 361 fibroblasts in mono-culture, then cells were co-cultured. In mono-culture of both cell types,  
 362 chitosan/HA NP showed a more rapid internalization, however eventually reaching a plateau,  
 363 as already seen in previous works (Lallana et al., 2017; Rios de la Rosa et al., 2017a). At the  
 364 later time points the fluorescence intensities produced by the siRNA were comparable in both  
 365 carriers (Figure 3). Qualitatively, in co-culture we observed a similar kinetic behavior, i.e. an  
 366 earlier plateau for chitosan/HA. However, assuming that the siRNA fluorescence always  
 367 provides quantitative and comparable estimates of NP internalization, we noticed another  
 368 more interesting phenomenon: in mono-culture the uptake in HDFa and HCT-116 appeared to  
 369 be comparable (Figure 3a) between the tested NP, whilst in co-culture HCT-116 always

370 internalized NP in much larger amounts (Figure 3b). Of note, where internalization in HCT-  
 371 116 always increased in co-culture, the internalization in HDFa increased for Nanocin/HA  
 372 and decreased for chitosan/HA, which means that although this HCT-116/HDFa differential  
 373 internalization (and targeting) was clear for both NP, it was much larger with chitosan/HA  
 374 systems. Mechanistically, this may be due an increased expression of CD44 and/or its  
 375 variants: we have demonstrated that the overall CD44 expression depends on the HCT-116  
 376 environment (3D culture increasing it) (Rios De La Rosa et al., 2018), whereas interactions  
 377 with cancer associated fibroblasts have been reported to increase CD44v expression in colon  
 378 cancer cells (Misra et al., 2011). Therapeutically, this is a very promising result, which  
 379 indicates that HA-coated formulations may be able to preferentially target and treat  
 380 populations of tumoral cells, thereby effectively reducing potential off-target effects.  
 381 Additionally, preliminary toxicology results showed no cytotoxicity (see Supplementary  
 382 Information, section SI.10 and Figure 5SI) or increased levels of cellular stress (see  
 383 Supplementary Information, section SI.11 and Figure 6SI). These results indicate that both  
 384 nanoparticles are suitable for further *in vivo* studies.

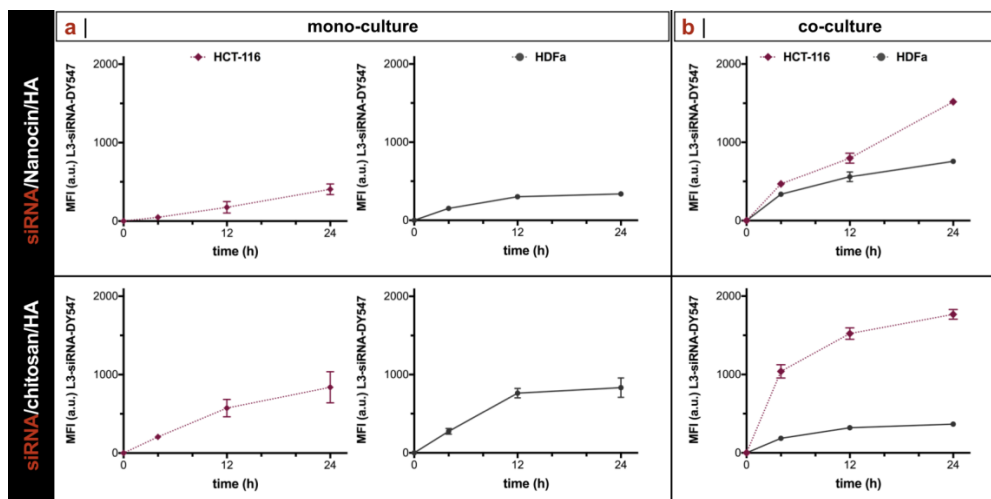


**Figure 3.** Kinetics of internalization of HA-coated L3-DY547-NP in CD44-expressing cell lines: cancer (HCT-116, CD44<sup>+</sup>, CD44v6<sup>high</sup>) and fibroblasts (HDF, CD44<sup>low</sup>). Results are expressed as mean  $\pm$  st.dev. of 10,000 events ( $n=3$  independent samples) at each time point. In mono-culture, similar kinetics of uptake are observed in both cell lines and for both NP. Whereas, a more tumor-like environment (co-culture of HCT-116 and HDFa) promotes a higher internalization of HA-coated NP, with increased uptake in cancer cells rather than fibroblasts at each time point (fold increase of 2-3 at the endpoint).

385 *3.2.3 Intracellular localization.* At a very early time point (1 h), despite the different  
386 internalization kinetics recorded through flow cytometry, chitosan/HA and Nanocin/HA NP  
387 did not showed a markedly different behavior: both of them were internalized in similar  
388 amounts with some, possibly initial signs of colocalization with lysosomal compartments  
389 (Figure 4a). This snapshot evidenced initial NP localization in lysosomes (yellow from  
390 contemporaneous emission of LysoTracker (green, 488nm) and siRNA (red, 561 nm), but also  
391 signs of possible escape (red siRNA signal around or flanking the yellow or green  
392 organelles). At 24 h, the two HA-decorated L3-DY547-NP are internalized/accumulated in  
393 HCT-116 in similar amounts (Figure 4b; n=5 fields of view, average of 150 cells observed for  
394 each treatment), which is broadly in line with the flow cytometry results. Of note, the siRNA  
395 cytosolic distribution seemed to be consistently more homogeneous with chitosan/HA NP,  
396 and more compartmented (visibly brighter spots) with Nanocin/HA NP. This phenomenon  
397 may indicate a possibly lower availability of siRNA in the Nanocin/HA at this stage, which  
398 would stem from a tighter complexation of the nucleic acid with the polycation. This tight  
399 interaction would be possibly caused by: a) the higher charge density on Nanocin and b) its  
400 lower size. The higher charge density of the polycation may cause a higher avidity; a more  
401 compact siRNA/polycation complex is possibly obtained with Nanocin (smaller Mw) that has  
402 an easier complexation compared to the larger polyelectrolytes (chitosan, entropic penalty for  
403 surface siRNA/polycation coupling) However, we should also consider that any factor  
404 increasing the complexation strength, such as a high charge density, is not necessarily  
405 detrimental: for example, using chitosan we have recently demonstrated that high density of  
406 amines increased chitosan binding to RNAs, but this effect was most likely overcome by  
407 higher endosomolytic efficiency (Lallana et al., 2017).

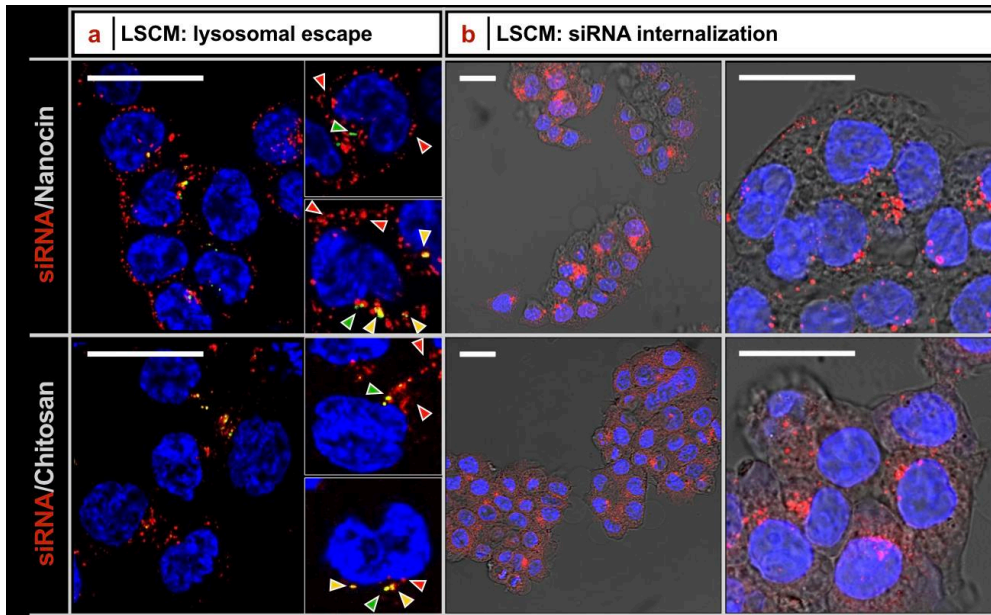


**Figure 4.** Nanoparticle and siRNA intracellular localization: a) lysosomal escape after 1 h incubation with NP, the arrows indicate lysosomes (green), the co-localization of nanoparticles in late endosomes/lysosomes (yellow) and released siRNA (red); b) internalization of siRNA in HCT-116 cells after 24 h incubation with NP, notably a similar percentage of siRNA was delivered in HCT-116, being 3.35% and 3.55% respectively for Nanocin/HA and chitosan/HA NP; a more ‘cloudy’ siRNA signal was observed in HCT-116 cells incubated with chitosan/HA NP, compared to a more localized siRNA signal for the Nanocin/HA counterparts. Scale bars: 25  $\mu$ m.

### 408 3.3 Silencing efficacy: siRNA release from nanoparticles and mRNA-KRAS knock-down

409 3.3.1 *Choice of siRNA.* We have first investigated the silencing efficiency of a panel of  
 410 different siRNA, employing simple Nanocin/siRNA polyplexes, since their high positive  
 411 charge (see Table 1) was supposed to stimulate the highest transfection. The silencing  
 412 efficiency was evaluated with qRT-PCR, rather than immunostaining methods, due to its  
 413 superior sensitivity; this is critical in KRAS analysis as the level of gene expression is low  
 414 and therefore difficult to detect. We eventually selected the  
 415 GGACUCUGAAGAUGUACCUAGGUACAUCUUCAGAGUCCs sequence as a promising  
 416 and more reproducible candidate for further experiments, after comparison of the silencing  
 417 efficiencies of 14 siRNAs targeting different regions within the mRNA sequences (see  
 418 Supplementary Information, section SI.2 and Figure 1SI).

419

420 3.3.2. *KRAS-silencing.* Chitosan/HA NP resulted in KRAS silencing to a level comparable to  
 421 the gold standard transfecting agent Lipofectamine (no statistical difference between the two

422 treatments at 48 h, Figure 5a); more importantly, the mRNA-KRAS reduction was  
 423 approximately 2-fold higher than with Nanocin/HA. As anticipated in section 3.2.3, the  
 424 higher charge density of Nanocin may be a limiting factor for siRNA intracellular availability,  
 425 which is a possible explanation for its lower silencing activity. Of interest, the HA-decorated  
 426 NP caused levels of silencing similar to those of the binary polyplexes, i.e. siRNA/polycation  
 427 only (see Supplementary Information, Figure 2SI); the latter are cationic species, and as such  
 428 are characterized by an efficient cell adhesion and penetration, therefore it is remarkable that  
 429 HA, most likely through its interactions with CD44, allows to overcome the effect of charge  
 430 inversion.

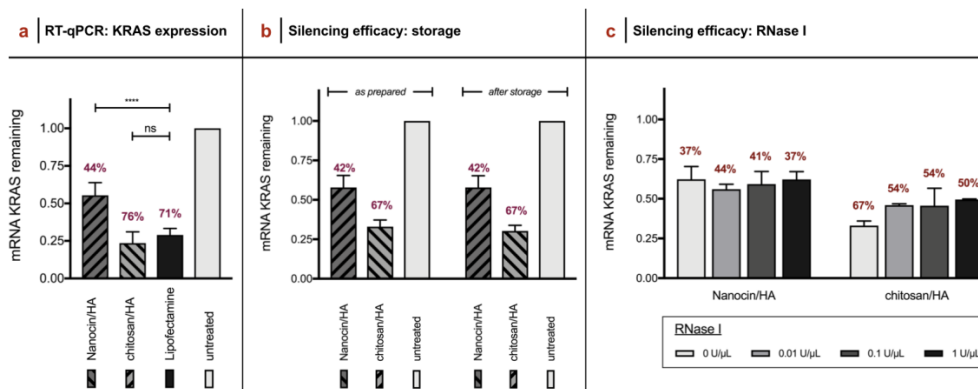


**Figure 5.** KRAS silencing efficacy of HA-coated NP. Relative KRAS expression and mRNA silencing was measured after 48 h treatment in HCT-116 cells with: a) *as prepared* NP: results show no statistical difference of chitosan-nanoparticles with respect to lipofectamine and a significant difference between Nanocin NP and lipofectamine ( $n=5$ ,  $p<0.0001$ ); b) NP after one-week storage at 4°C generally showed a silencing efficacy similar to that of *as prepared* NP. Data are expressed as percentage with respect to untreated cells and are the average on  $n=3$  independent experiments. Lipofectamine was used as control (data not reported); c) NP exposed (incubation prior use) to RNase I at different concentrations (0, 0.01, 0.1, 1 U/μL). Data are expressed as percentage with respect to untreated cells and are the average on  $n=3$  independent experiments. Lipofectamine was used as control (data not reported).

431 **3.3.3 Effect of storage on silencing efficacy.** NP were also stored for 1 week at 4°C in  
 432 deionized water before using them in silencing experiments; this storage period caused no  
 433 significant alteration in the silencing activity of both NP (Figure 5b). Interestingly, we  
 434 observed that without HA (direct complexation between siRNA and polycations) the  
 435 chitosan-based NP experienced a significant reduction in silencing performance (from >60%  
 436 to about 40%, Supplementary Information Figure SI2), which is likely to ascribe to the low

437 degree of protonation of chitosan amines, which eventually allows self-aggregation of the  
438 polymer and physical destabilization of the particles.

439

440 *3.3.3 Effect of RNase I exposure on silencing performance.* As a last step in the assessment of  
441 NP for *in vivo* administration, we tested whether siRNA loaded in Nanocin- and chitosan-NP  
442 could preserve its silencing functionality when the NP are exposed to potentially RNA-  
443 degrading condition, such as the presence of RNase. To support our previous demonstration  
444 that the apparent integrity of the loaded siRNA (Figure 1e) ensures the preservation of its  
445 silencing capacity, we further tested the silencing efficiency of both NP after exposure to  
446 different concentration of RNase I (i.e. 0.01, 0.1, 1 U/ $\mu$ L) and compared the results to non-  
447 exposed NP (incubated in nuclease free water, control). In these experiments, concentrations  
448 of RNase up to 1 U/ $\mu$ L did not alter the performance of Nanocin/HA NP, whereas that of  
449 chitosan/HA NP was in part decreased. This can be ascribed to the higher complexation  
450 strength of Nanocin (higher charge density, lower molecular weight), which makes more  
451 difficult for an enzyme to reach its target in the bulk of a particle. Indeed, similar effects can  
452 be seen also for the polycomplexes formed without HA (see Supplementary information,  
453 Figure 3SI).

#### 454 **Conclusions**

455 We compared two HA-based polyplex systems for the delivery of siRNA in CD44<sup>+</sup> cell lines  
456 (HCT-116 and HDFa), for a perspective KRAS-targeted tumor therapy. Our main findings are  
457 that: a) CD44<sup>high</sup>/CD44<sup>v+</sup> cancer cells (HCT-116) are more active for the internalization of  
458 HA-coated NP than stromal standard CD44<sup>+</sup> cells (HDFa), and that this difference amplifies  
459 when cells are co-cultured. This is a very encouraging finding that supports the use of HA for  
460 tumor targeting, with potential low off-target effects; b) the strength of the polyelectrolyte  
461 complexation is an important parameter that carries a delicate balance of favorable and  
462 detrimental effects. The stronger interactions between Nanocin and siRNA (and HA) appear  
463 to negatively affect the silencing efficacy of such NP, possibly due to the lower availability of

464 the nucleic acid. On the other hand, they most likely provide a higher stability against  
465 nucleases (and other harmful agents for the nucleic acid). Remarkably, we found that chitosan  
466 NP presented the right compromise between polyplexes stability and avidity/efficiency of  
467 siRNA release, which conferred them a high silencing efficacy comparable to the gold  
468 standard transfecting agent (i.e. Lipofectamine). With this rationale, further *in vivo* studies will  
469 need to demonstrate whether the different complexation also affects the stability of the NP in  
470 the blood stream, and whether the higher silencing capacity of chitosan-based systems can be  
471 confirmed in real tumors.

#### 472 **Acknowledgement**

473 The NorthWest Centre of Advanced Drug Delivery (NoWCADD) established at the  
474 University of Manchester in collaboration with AstraZeneca. Dr Enrique Lallana and Dr Julio  
475 Rios de La Rosa are gratefully acknowledged for both discussions and experimental help. The  
476 Bioimaging Facility of the Faculty of Life Sciences (University of Manchester) is maintained  
477 with grants from BBSRC, Wellcome Trust, and the University of Manchester Strategic Fund.  
478 This work was funded by the Innovate UK project number 101710.

479



480 **References**

- 481 Almalik, A., Day, P.J., Tirelli, N., 2013a. HA-coated chitosan nanoparticles for CD44-  
482 mediated nucleic acid delivery. *Macromol. Biosci.* 13, 1671–1680.  
483 <https://doi.org/10.1002/mabi.201300302>
- 484 Almalik, A., Karimi, S., Ouasti, S., Donno, R., Wandrey, C., Day, P.J., Tirelli, N., 2013b.  
485 Hyaluronic acid (HA) presentation as a tool to modulate and control the receptor-  
486 mediated uptake of HA-coated nanoparticles. *Biomaterials* 34, 5369–5380.  
487 <https://doi.org/10.1016/j.biomaterials.2013.03.065>
- 488 Alves, S., Castro, L., Fernandes, M.S., Francisco, R., Castro, P., Priault, M., Chaves, S.R.,  
489 Moyer, M.P., Oliveira, C., Seruca, R., Corte-Real, M., Sousa, M.J., Preto, A., 2015.  
490 Colorectal cancer-related mutant KRAS alleles function as positive regulators of  
491 autophagy. *Oncotarget* 6, 30787–30802. <https://doi.org/10.18632/oncotarget.5021>
- 492 Appels, N., Beijnen, J., Schellens, J., 2005. Development of Farnesyl Transferase Inhibitors:  
493 A Review. *Oncologist* 10, 565–578. <https://doi.org/10.1634/theoncologist.10-8-565>
- 494 Asati, V., Mahapatra, D.K., Bharti, S.K., 2017. K-Ras and its inhibitors towards personalized  
495 cancer treatment: Pharmacological and structural perspectives. *Eur. J. Med. Chem.*  
496 <https://doi.org/10.1016/j.ejmech.2016.09.049>
- 497 Auzenne, E., Ghosh, S.C., Khodadadian, M., Rivera, B., Farquhar, D., Price, R.E., Ravoori,  
498 M., Kundra, V., Freedman, R.S., Klostergaard, J., 2007. Hyaluronic Acid- Paclitaxel:  
499 Antitumor Efficacy against CD44(+) Human Ovarian Carcinoma Xenografts. *Neoplasia*  
500 9, 479–486. <https://doi.org/10.1593/NEO.07229>
- 501 Bassi, P.F., Volpe, A., D'Agostino, D., Palermo, G., Renier, D., Franchini, S., Rosato, A.,  
502 Racioppi, M., 2011. Paclitaxel-hyaluronic acid for intravesical therapy of bacillus  
503 calmette-gurin refractory carcinoma in situ of the bladder: Results of a phase i study. *J.*  
504 *Urol.* 185, 445–449. <https://doi.org/10.1016/j.juro.2010.09.073>
- 505 Birzele, F., Voss, E., Nopora, A., Honold, K., Heil, F., Lohmann, S., Verheul, H., Le  
506 Tourneau, C., Delord, J.P., Van Herpen, C., Mahalingam, D., Coveler, A.L., Meresse,

507 V., Weigand, S., Runza, V., Cannarile, M., 2015. CD44 Isoform status predicts response  
508 to treatment with Anti-CD44 antibody in cancer patients. *Clin. Cancer Res.* 21, 2753–  
509 2762. <https://doi.org/10.1158/1078-0432.CCR-14-2141>

510 Blasco, R.B., Francoz, S., Santamaría, D., Cañamero, M., Dubus, P., Charron, J., Baccarini,  
511 M., Barbacid, M., 2011. C-Raf, but Not B-Raf, Is Essential for Development of K-Ras  
512 Oncogene-Driven Non-Small Cell Lung Carcinoma. *Cancer Cell* 19, 652–663.  
513 <https://doi.org/10.1016/j.ccr.2011.04.002>

514 Chin, L., Tam, A., Pomerantz, J., Wong, M., Holash, J., Bardeesy, N., Shen, Q., O'Hagan, R.,  
515 Pantginis, J., Zhou, H., Horner, J.W., Cordon-Cardo, C., Yancopoulos, G.D., DePinho,  
516 R.A., 1999. Essential role for oncogenic ras in tumour maintenance. *Nature* 400, 468–  
517 472. <https://doi.org/10.1038/22788>

518 Chindera, K., Mahato, M., Kumar Sharma, A., Horsley, H., Kloc-Muniak, K.,  
519 Kamaruzzaman, N.F., Kumar, S., McFarlane, A., Stach, J., Bentin, T., Good, L., 2016.  
520 The antimicrobial polymer PHMB enters cells and selectively condenses bacterial  
521 chromosomes. *Sci. Rep.* 6, 23121. <https://doi.org/10.1038/srep23121>

522 Collins, M.A., Bednar, F., Zhang, Y., Brisset, J.-C., Galbán, S., Galbán, C.J., Rakshit, S.,  
523 Flannagan, K.S., Adsay, N.V., Pasca di Magliano, M., Pasca, M., 2012. Oncogenic Kras  
524 is required for both the initiation and maintenance of pancreatic cancer in mice. *J. Clin.*  
525 *Invest.* 122, 639–653. <https://doi.org/10.1172/JCI59227DS1>

526 Collisson, E.A., Trejo, C.L., Silva, J.M., Gu, S., Korkola, J.E., Heiser, L.M., Charles, R.P.,  
527 Rabinovich, B.A., Hann, B., Dankort, D., Spellman, P.T., Phillips, W.A., Gray, J.W.,  
528 McMahon, M., 2012. A Central role for RAF→MEK→ERK signaling in the genesis of  
529 pancreatic ductal adenocarcinoma. *Cancer Discov.* 2, 685–693.  
530 <https://doi.org/10.1158/2159-8290.CD-11-0347>

531 Coradini, D., Pellizzaro, C., Miglierini, G., Daidone, M.G., Perbellini, A., 1999. Hyaluronic  
532 acid as drug delivery for sodium butyrate: Improvement of the anti-proliferative activity  
533 on a breast-cancer cell line. *Int. J. Cancer* 81, 411–416.  
534 [https://doi.org/10.1002/\(SICI\)1097-0215\(19990505\)81:3<411::AID-IJC15>3.0.CO;2-F](https://doi.org/10.1002/(SICI)1097-0215(19990505)81:3<411::AID-IJC15>3.0.CO;2-F)

535 Cox, A.D., Fesik, S.W., Kimmelman, A.C., Luo, J., Der, C.J., 2014. Drugging the  
536 undruggable RAS: Mission Possible? *Nat. Rev. Drug Discov.*  
537 <https://doi.org/10.1038/nrd4389>

538 Culty, M., Nguyen, H.A., Underhill, C.B., 1992. The hyaluronan receptor (CD44) participates  
539 in the uptake and degradation of hyaluronan. *J. Cell Biol.* 116, 1055–1062.  
540 <https://doi.org/10.1083/jcb.116.4.1055>

541 Deng, X., Cao, M., Zhang, J., Hu, K., Yin, Z., Zhou, Z., Xiao, X., Yang, Y., Sheng, W., Wu,  
542 Y., Zeng, Y., 2014. Hyaluronic acid-chitosan nanoparticles for co-delivery of MiR-34a  
543 and doxorubicin in therapy against triple negative breast cancer. *Biomaterials* 35, 4333–  
544 4344. <https://doi.org/10.1016/J.BIOMATERIALS.2014.02.006>

545 Ellis, C.A., Clark, G., 2000. The importance of being K-Ras. *Cell. Signal.*  
546 [https://doi.org/10.1016/S0898-6568\(00\)00084-X](https://doi.org/10.1016/S0898-6568(00)00084-X)

547 Ganesh, S., Iyer, A.K., Morrissey, D. V., Amiji, M.M., 2013. Hyaluronic acid based self-  
548 assembling nanosystems for CD44 target mediated siRNA delivery to solid tumors.  
549 *Biomaterials* 34, 3489–3502. <https://doi.org/10.1016/j.biomaterials.2013.01.077>

550 Hatzivassiliou, G., Haling, J.R., Chen, H., Song, K., Price, S., Heald, R., Hewitt, J.F.M., Zak,  
551 M., Peck, A., Orr, C., Merchant, M., Hoeflich, K.P., Chan, J., Luoh, S.M., Anderson,  
552 D.J., Ludlam, M.J.C., Wiesmann, C., Ultsch, M., Friedman, L.S., Malek, S., Belvin, M.,  
553 2013. Mechanism of MEK inhibition determines efficacy in mutant KRAS- versus  
554 BRAF-driven cancers. *Nature* 501, 232–236. <https://doi.org/10.1038/nature12441>

555 Janes, K.A., Fresneau, M.P., Marazuela, A., Fabra, A., Alonso, M.J., 2001. Chitosan  
556 nanoparticles as delivery systems for doxorubicin. *J. Control. Release* 73, 255–267.  
557 [https://doi.org/10.1016/S0168-3659\(01\)00294-2](https://doi.org/10.1016/S0168-3659(01)00294-2)

558 Kamerkar, S., Lebleu, V.S., Sugimoto, H., Yang, S., Ruivo, C.F., Melo, S.A., Lee, J.J.,  
559 Kalluri, R., 2017. Exosomes facilitate therapeutic targeting of oncogenic KRAS in  
560 pancreatic cancer. *Nature* 546, 498–503. <https://doi.org/10.1038/nature22341>

561 Karousou, E., Misra, S., Ghatak, S., Dobra, K., Götte, M., Vigetti, D., Passi, A., Karamanos,  
562 N.K., Skandalis, S.S., 2017. Roles and targeting of the HAS/hyaluronan/CD44

563 molecular system in cancer. *Matrix Biol.* <https://doi.org/10.1016/j.matbio.2016.10.001>

564 Kim, H., Yang, X.L., Rosada, C., Hamilton, S.R., August, J.T., 1994. CD44 expression in  
565 colorectal adenomas is an early event occurring prior to K-ras and p53 gene mutation.  
566 *Arch. Biochem. Biophys.* <https://doi.org/10.1006/abbi.1994.1199>

567 Lallana, E., Rios de la Rosa, J.M., Tirella, A., Pelliccia, M., Gennari, A., Stratford, I.J., Puri,  
568 S., Ashford, M., Tirelli, N., 2017. Chitosan/Hyaluronic Acid Nanoparticles: Rational  
569 Design Revisited for RNA Delivery. *Mol. Pharm.* 14, 2422–2436.  
570 <https://doi.org/10.1021/acs.molpharmaceut.7b00320>

571 Li, F., Park, S.-J., Ling, D., Park, W., Han, J.Y., Na, K., Char, K., 2013. Hyaluronic acid-  
572 conjugated graphene oxide/photosensitizer nanohybrids for cancer targeted  
573 photodynamic therapy. *J. Mater. Chem. B* 1, 1678. <https://doi.org/10.1039/c3tb00506b>

574 Luo, Y., Bernshaw, N.J., Lu, Z., Kopecek, J., Prestwich, G.D., 2002. Targeted Delivery of  
575 Doxorubicin by HPMA Copolymer-Hyaluronan Bioconjugates. *Pharm. Res.* 19, 396–  
576 402. <https://doi.org/10.1023/A:1015170907274>

577 Ma, M., Chen, H., Chen, Y., Zhang, K., Wang, X., Cui, X., Shi, J., 2012. Hyaluronic acid-  
578 conjugated mesoporous silica nanoparticles: excellent colloidal dispersity in  
579 physiological fluids and targeting efficacy. *J. Mater. Chem.* 22, 5615.  
580 <https://doi.org/10.1039/c2jm15489g>

581 Mao, S., Shuai, X., Unger, F., Simon, M., Bi, D., Kissel, T., 2004. The depolymerization of  
582 chitosan: Effects on physicochemical and biological properties. *Int. J. Pharm.* 281, 45–  
583 54. <https://doi.org/10.1016/j.ijpharm.2004.05.019>

584 Mattheolabakis, G., Milane, L., Singh, A., Amiji, M.M., 2015. Hyaluronic acid targeting of  
585 CD44 for cancer therapy: From receptor biology to nanomedicine. *J. Drug Target.* 23,  
586 605–618. <https://doi.org/10.3109/1061186X.2015.1052072>

587 Misra, S., Hascall, V.C., Berger, F.G., Markwald, R.R., Ghatak, S., 2008. Hyaluronan, CD44,  
588 and cyclooxygenase-2 in colon cancer. *Connect. Tissue Res.*  
589 <https://doi.org/10.1080/03008200802143356>

590 Misra, S., Helden, P., Hascall, V.C., Karamanos, N.K., Skandalis, S.S., Markwald, R.R.,

591 Ghatak, S., 2011. Hyaluronan-CD44 interactions as potential targets for cancer therapy.  
592 FEBS J. 278, 1429–1443. <https://doi.org/10.1111/j.1742-4658.2011.08071.x>

593 Parajó, Y., d'Angelo, I., Welle, A., Garcia-Fuentes, M., Alonso, M.J., 2010. Hyaluronic  
594 acid/Chitosan nanoparticles as delivery vehicles for VEGF and PDGF-BB. *Drug Deliv.*  
595 17, 596–604. <https://doi.org/10.3109/10717544.2010.509357>

596 Ponta, H., Sherman, L., Herrlich, P.A., 2003. CD44: From adhesion molecules to signalling  
597 regulators. *Nat. Rev. Mol. Cell Biol.* 4, 33–45. <https://doi.org/10.1038/nrm1004>

598 Rios de la Rosa, J.M., Tirella, A., Gennari, A., Stratford, I.J., Tirelli, N., 2017a. The CD44-  
599 Mediated Uptake of Hyaluronic Acid-Based Carriers in Macrophages. *Adv. Healthc.*  
600 *Mater.* 6. <https://doi.org/10.1002/adhm.201601012>

601 Rios de la Rosa, J.M., Tirella, A., Gennari, A., Stratford, I.J., Tirelli, N., 2017b. The CD44-  
602 Mediated Uptake of Hyaluronic Acid-Based Carriers in Macrophages. *Adv. Healthc.*  
603 *Mater.* 6, 1601012. <https://doi.org/10.1002/adhm.201601012>

604 Rios de la Rosa, J.M., Tirella, A., Tirelli, N., 2018. Receptor-Targeted Drug Delivery and the  
605 (Many) Problems We Know of: The Case of CD44 and Hyaluronic Acid. *Adv. Biosyst.*  
606 2, 1800049. <https://doi.org/10.1002/adbi.201800049>

607 Rios De La Rosa, J.M., Wubetu, J., Tirelli, N., Tirella, A., 2018. Colorectal tumor 3D in vitro  
608 models: advantages of biofabrication for the recapitulation of early stages of tumour  
609 development. *Biomed. Phys. Eng. Express* 17.

610 Ross, S.J., Revenko, A.S., Hanson, L.L., Ellston, R., Staniszewska, A., Whalley, N., Pandey,  
611 S.K., Revill, M., Rooney, C., Buckett, L.K., Klein, S.K., Hudson, K., Monia, B.P.,  
612 Zinda, M., Blakey, D.C., Lyne, P.D., Macleod, A.R., 2017. Targeting KRAS-dependent  
613 tumors with AZD4785, a high-affinity therapeutic antisense oligonucleotide inhibitor of  
614 KRAS. *Sci. Transl. Med.* 9, eaal5253. <https://doi.org/10.1126/scitranslmed.aal5253>

615 Shin, W., Lee, S.K., Hwang, J.H., Park, J.C., Cho, Y.H., Ro, E.J., Song, Y., Seo, H.R., Choi,  
616 K.Y., 2018. Identification of Ras-degrading small molecules that inhibit the  
617 transformation of colorectal cancer cells independent of  $\beta$ -catenin signaling. *Exp. Mol.*  
618 *Med.* 50, 71. <https://doi.org/10.1038/s12276-018-0102-5>

619 Stephen, A.G., Esposito, D., Bagni, R.G., McCormick, F., 2014. Dragging ras back in the  
620 ring. *Cancer Cell*. <https://doi.org/10.1016/j.ccr.2014.02.017>

621 Stylianopoulos, T., Jain, R.K., 2015. Design considerations for nanotherapeutics in oncology.  
622 *Nanomedicine Nanotechnology, Biol. Med.* <https://doi.org/10.1016/j.nano.2015.07.015>

623 Surace, C., Arpicco, S., Dufay-Wojcicki, A., Marsaud, V., Bouclier, C., Clay, D., Cattel, L.,  
624 Renoir, J.-M., Fattal, E., 2009. Lipoplexes Targeting the CD44 Hyaluronic Acid  
625 Receptor for Efficient Transfection of Breast Cancer Cells. *Mol. Pharm.* 6, 1062–1073.  
626 <https://doi.org/10.1021/mp800215d>

627 Überall, I., Kolář, Z., Trojanec, R., Berkovcová, J., Hajdúch, M., 2008. The status and role of  
628 ErbB receptors in human cancer. *Exp. Mol. Pathol.*  
629 <https://doi.org/10.1016/j.yexmp.2007.12.002>

630 Wang, Y., Kaiser, C.E., Frett, B., Li, H.Y., 2013. Targeting mutant KRAS for anticancer  
631 therapeutics: A review of novel small molecule modulators. *J. Med. Chem.* 56, 5219–  
632 5230. <https://doi.org/10.1021/jm3017706>

633 Yi Luo, †, Michael R. Ziebell, †,‡ and Glenn D. Prestwich\*, †, 2000. A Hyaluronic  
634 Acid–Taxol Antitumor Bioconjugate Targeted to Cancer Cells.  
635 <https://doi.org/10.1021/BM000283N>

636 Yu, M., Jambhrunkar, S., Thorn, P., Chen, J., Gu, W., Yu, C., 2013. Hyaluronic acid modified  
637 mesoporous silica nanoparticles for targeted drug delivery to CD44-overexpressing  
638 cancer cells. *Nanoscale* 5, 178–83. <https://doi.org/10.1039/c2nr32145a>

639 Zhang, Z., Jiang, G., Yang, F., Wang, J., 2006. Knockdown of mutant K-ras expression by  
640 adenovirus-mediated siRNA inhibits the in vitro and in vivo growth of lung cancer cells.  
641 *Cancer Biol. Ther.* 5, 1481–1486. <https://doi.org/10.4161/cbt.5.11.3297>

642 Zhao, P., Damerow, M.S., Stern, P., Liu, A.H., Sweet-Cordero, A., Siziopikou, K., Neilson,  
643 J.R., Sharp, P.A., Cheng, C., 2013. CD44 promotes Kras-dependent lung  
644 adenocarcinoma. *Oncogene* 32, 5186–5190. <https://doi.org/10.1038/onc.2012.542>

645 Zorde Khvalevsky, E., Gabai, R., Rachmut, I.H., Horwitz, E., Brunshwig, Z., Orbach, A.,  
646 Shemi, A., Golan, T., Domb, A.J., Yavin, E., Giladi, H., Rivkin, L., Simerzin, A.,

647 Eliakim, R., Khalaileh, A., Hubert, A., Lahav, M., Kopelman, Y., Goldin, E., Dancour,  
648 A., Hants, Y., Arbel-Alon, S., Abramovitch, R., Shemi, A., Galun, E., 2013. Mutant  
649 KRAS is a druggable target for pancreatic cancer. *Proc. Natl. Acad. Sci.* 110, 20723–  
650 20728. <https://doi.org/10.1073/pnas.1314307110>  
651

**Supplementary Information**

[Click here to download Supplementary Material: SI-rev 01 2019 v2.docx](#)



Figure 1

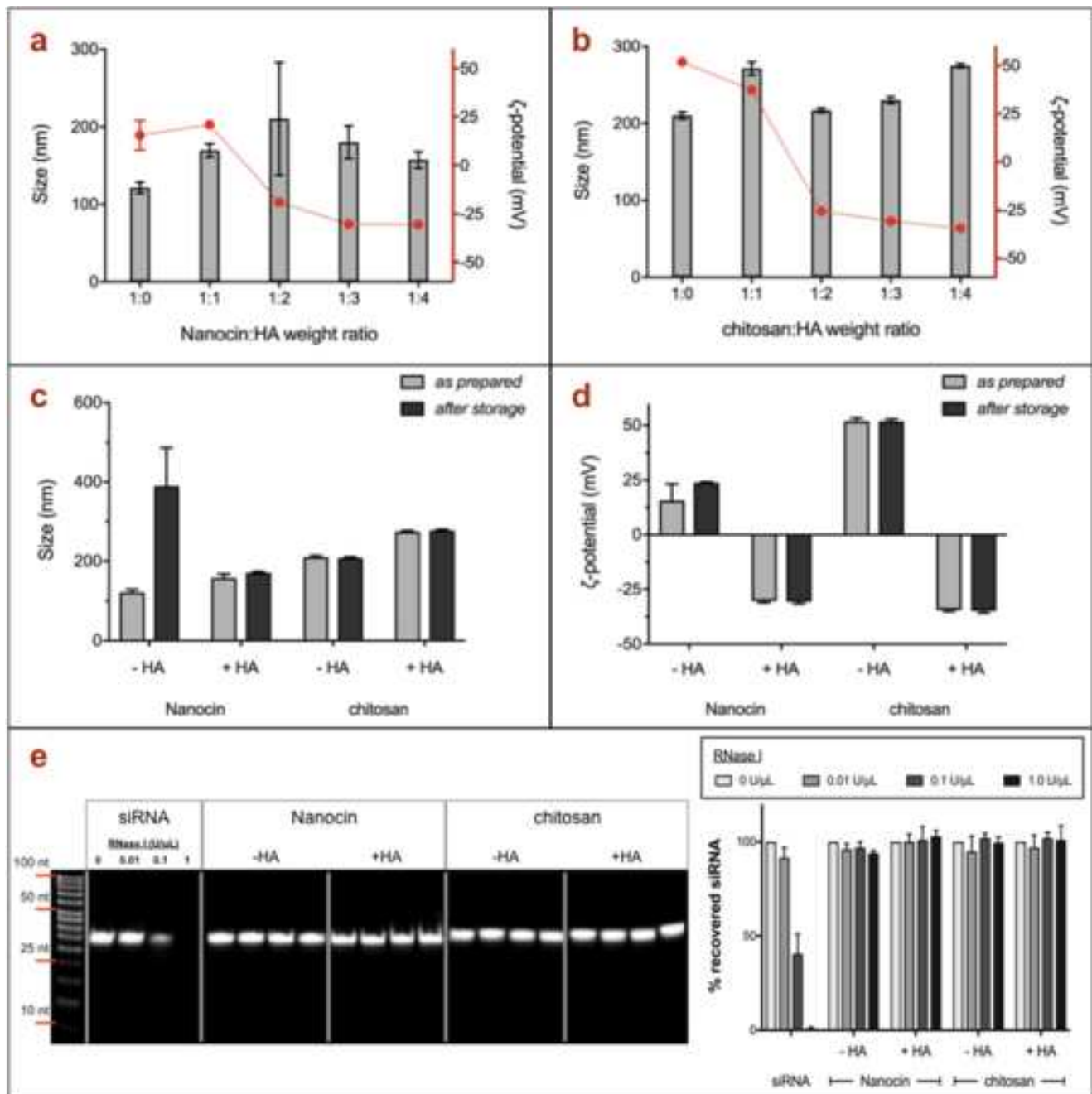


Figure 2

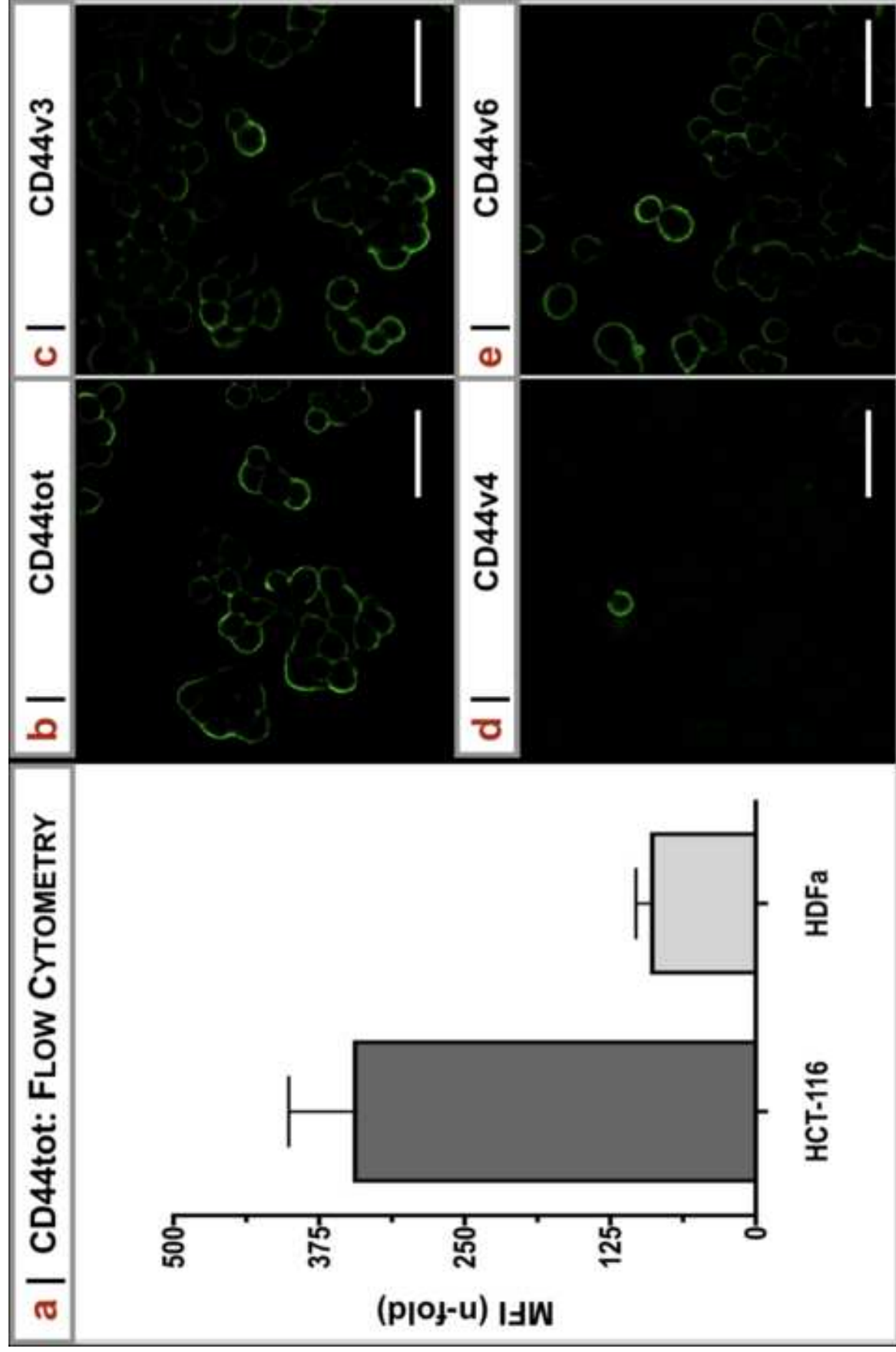


Figure 3

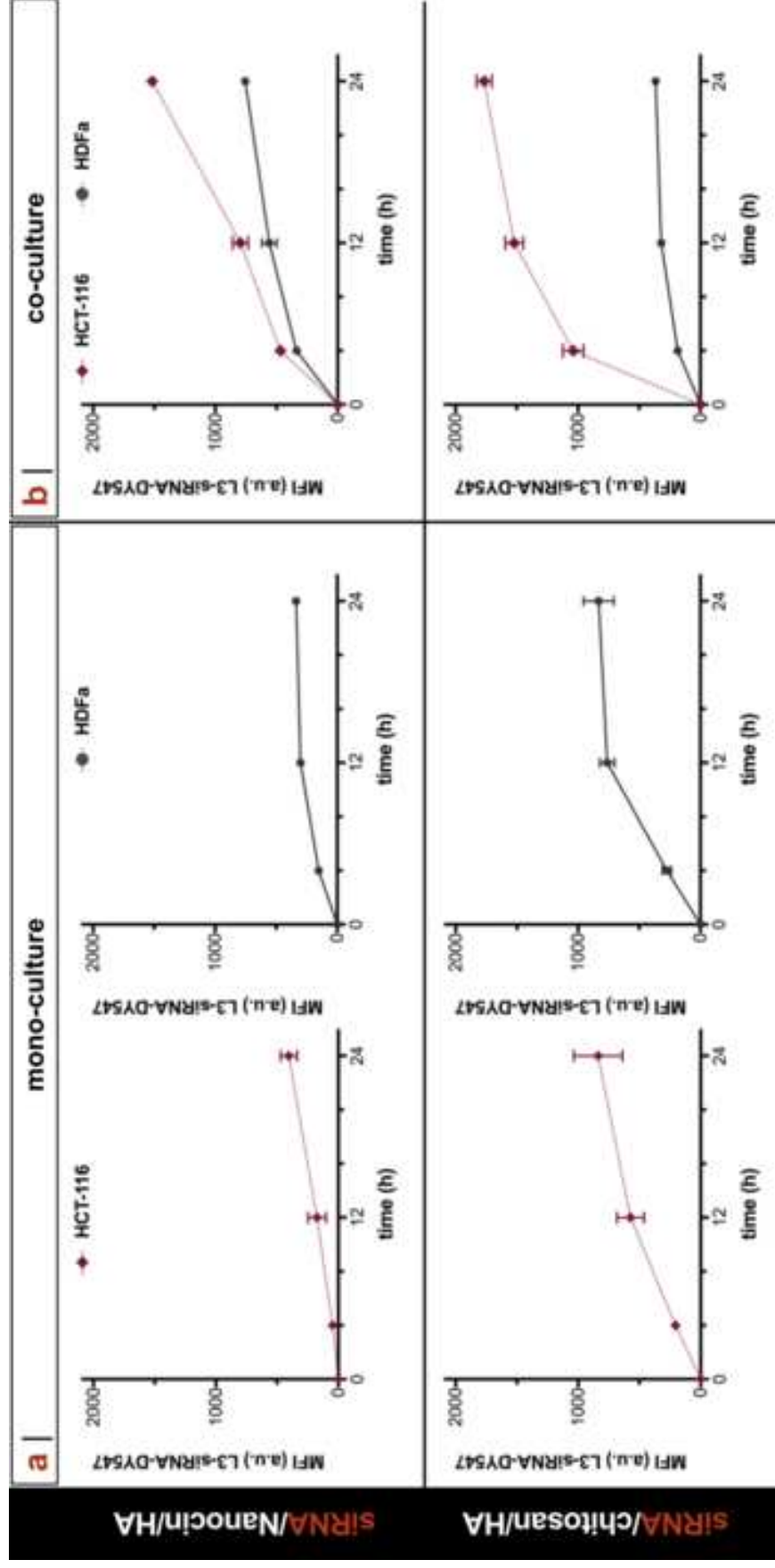


Figure 4

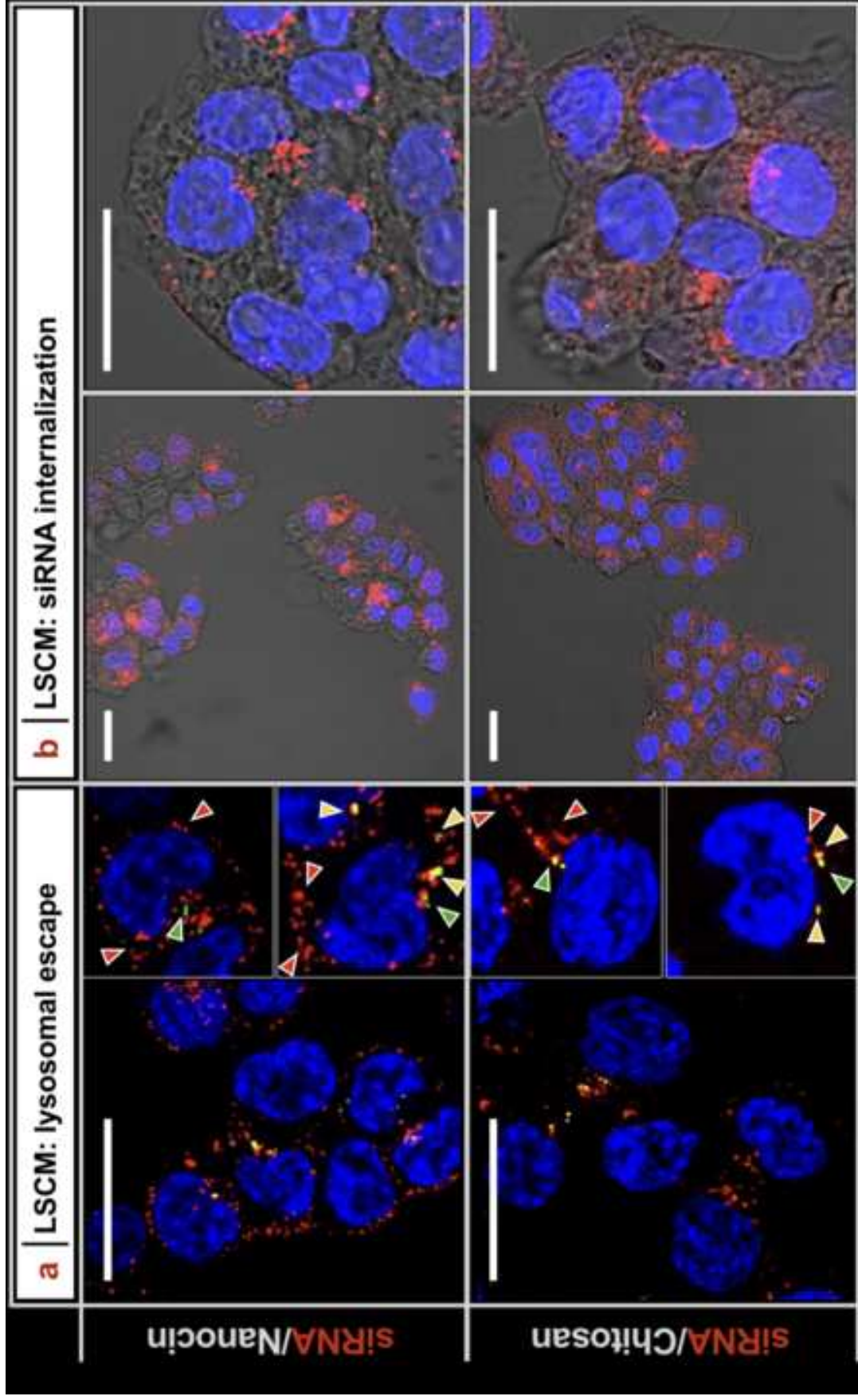
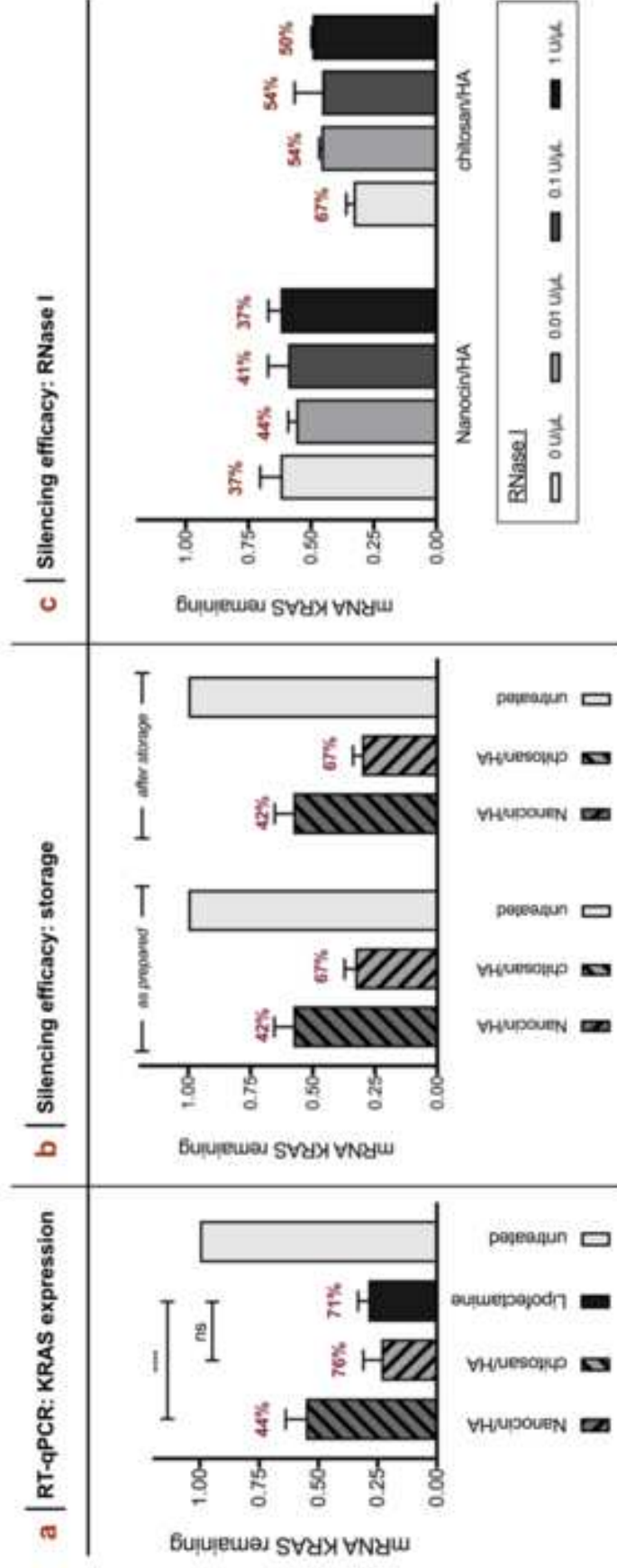


Figure 5



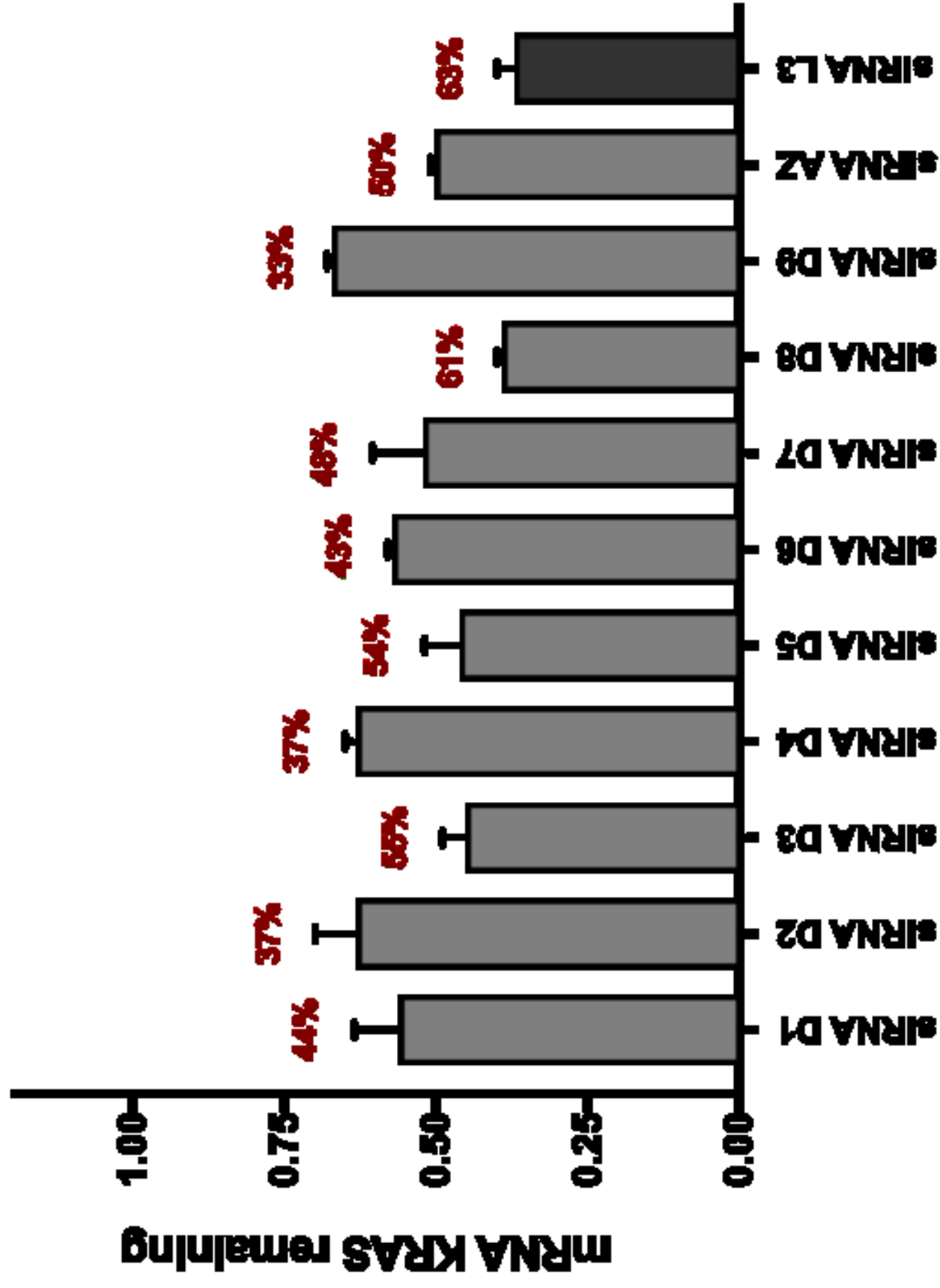


Figure S11

Figure S12

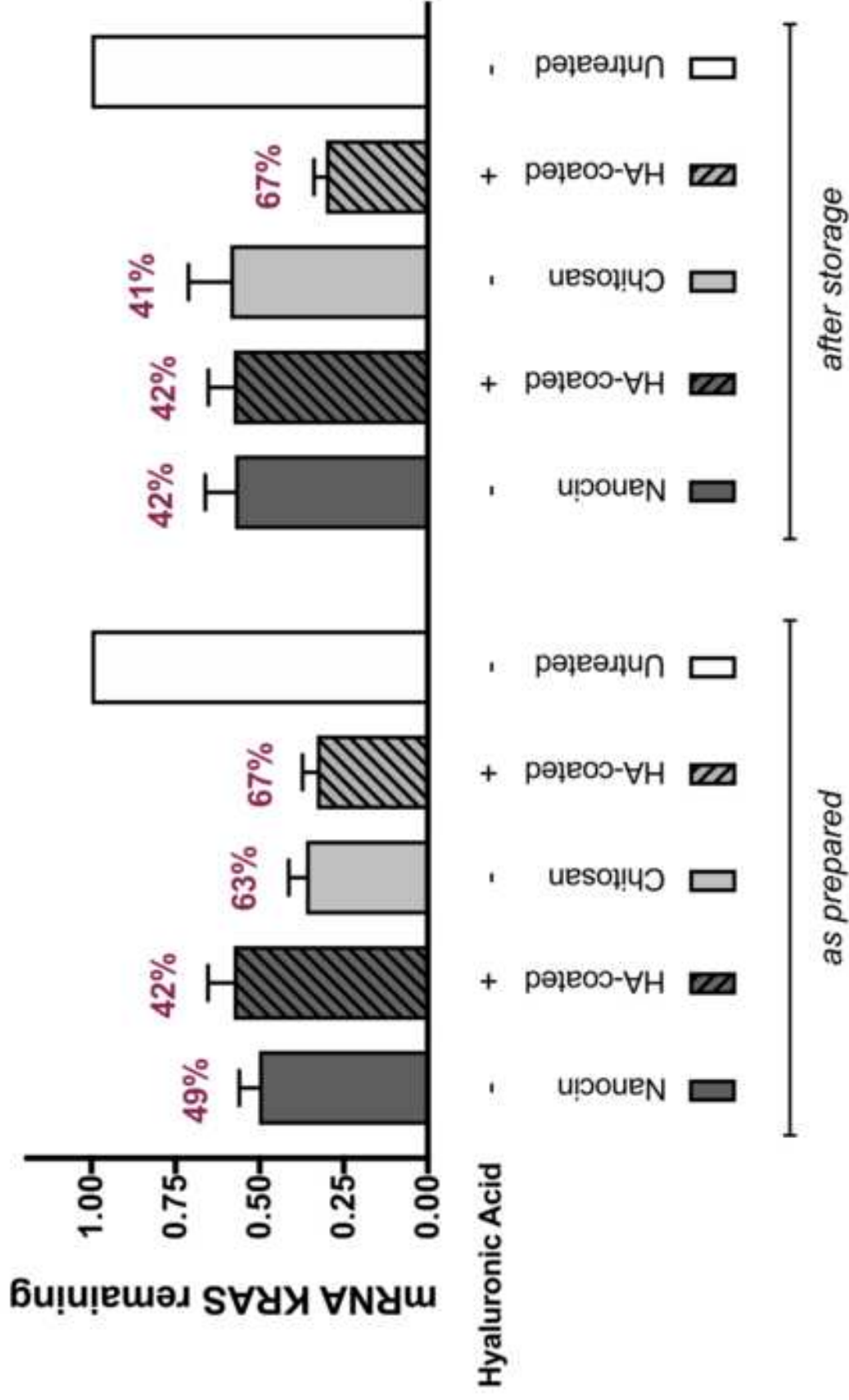


Figure S13

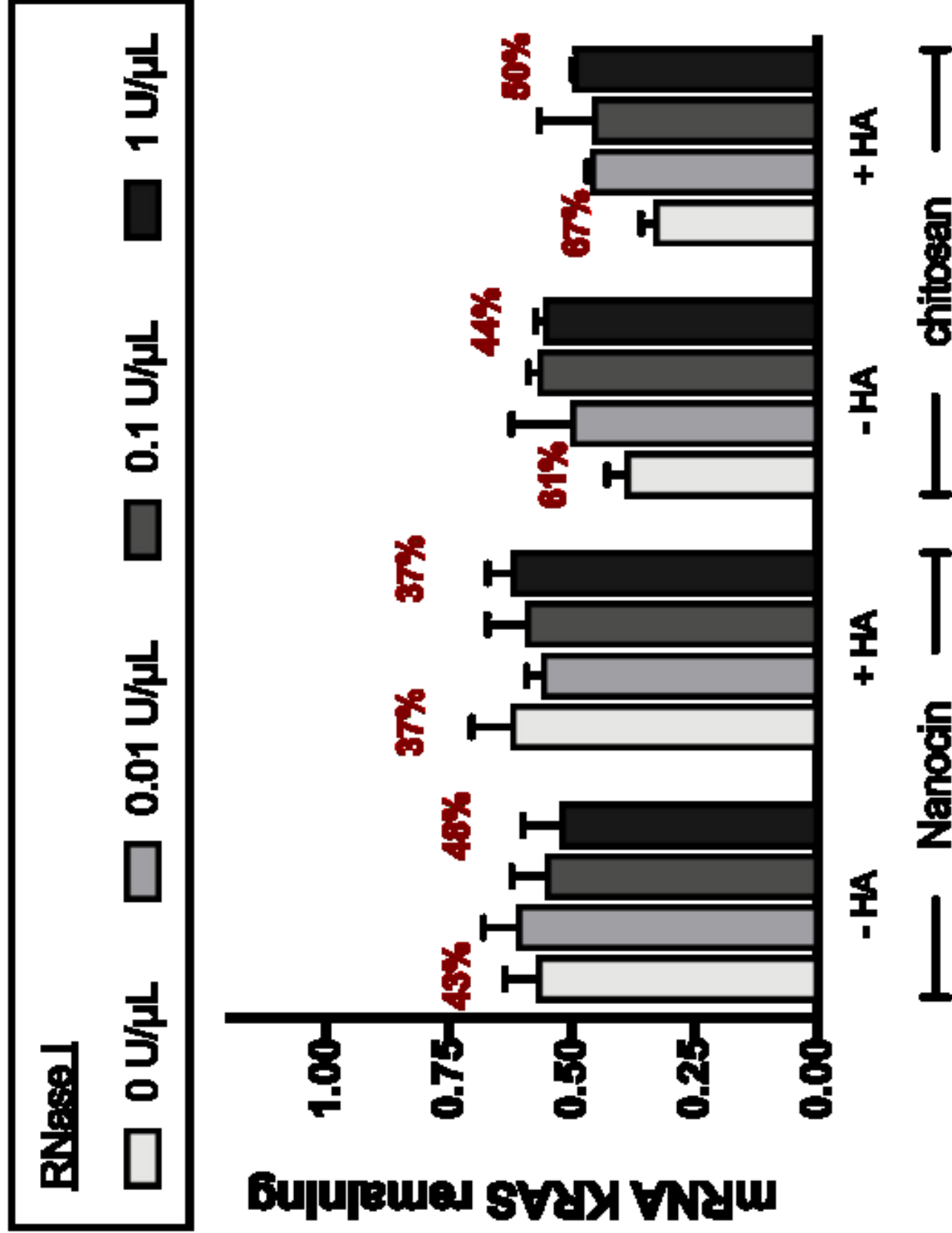




Figure S14

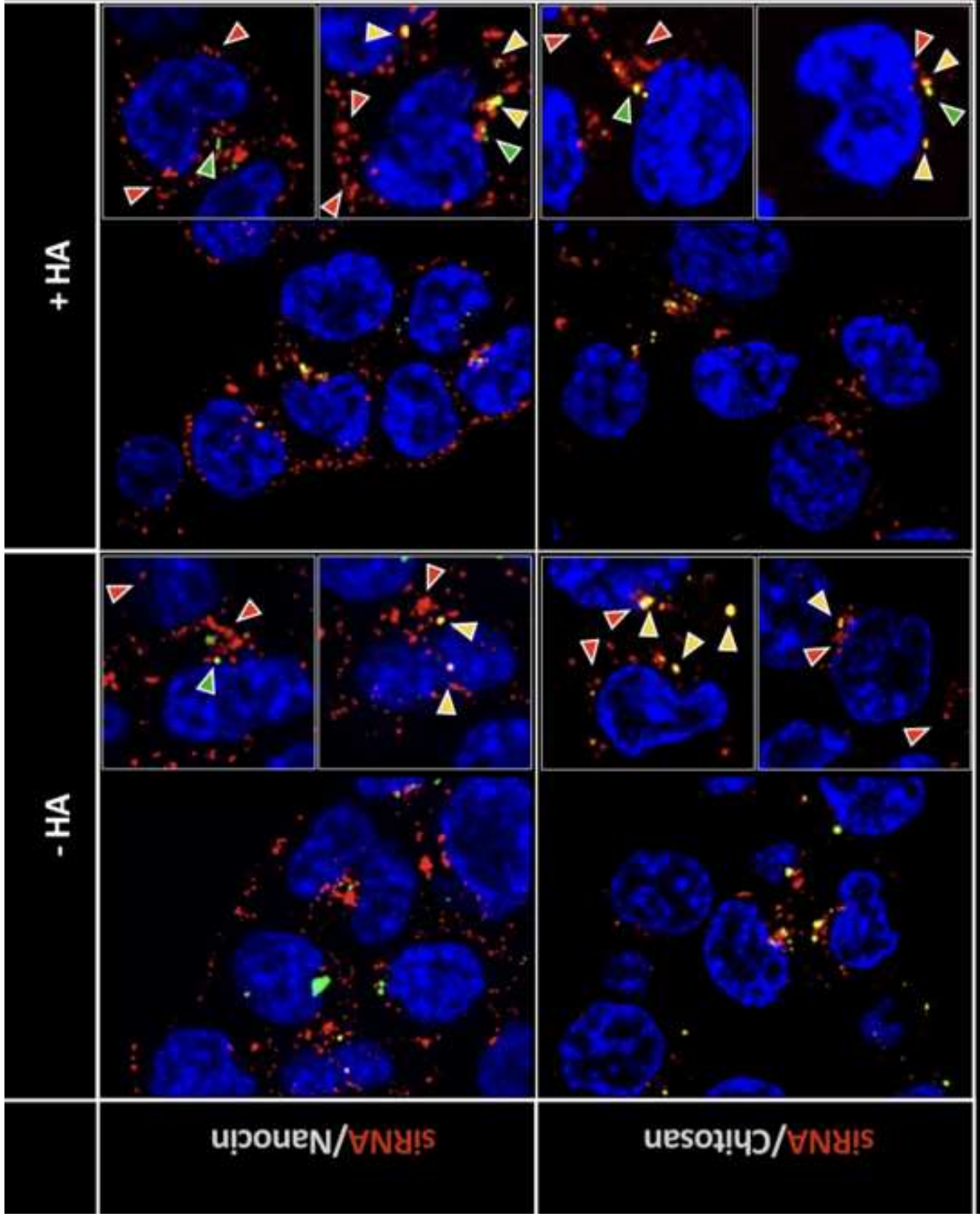
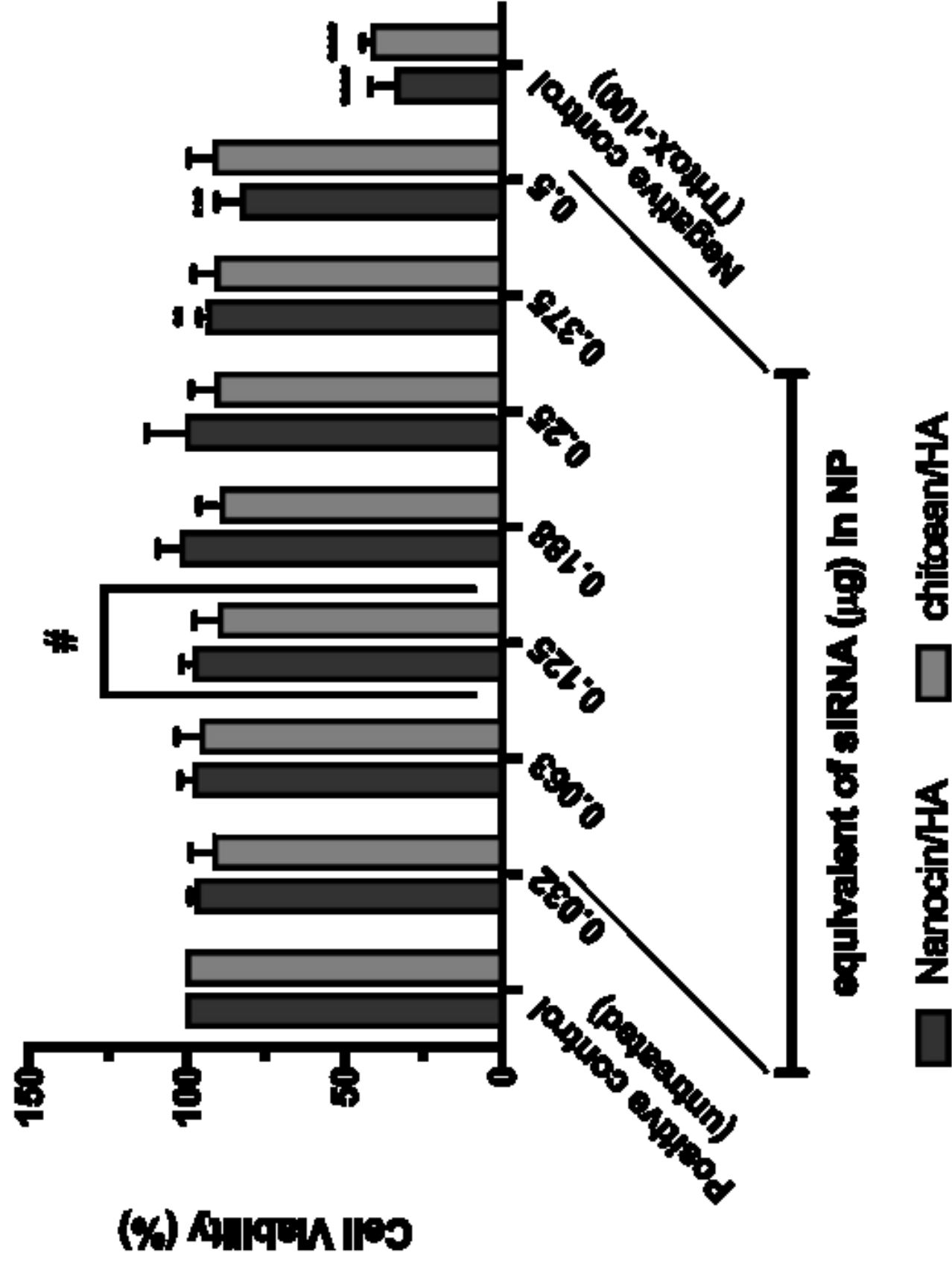
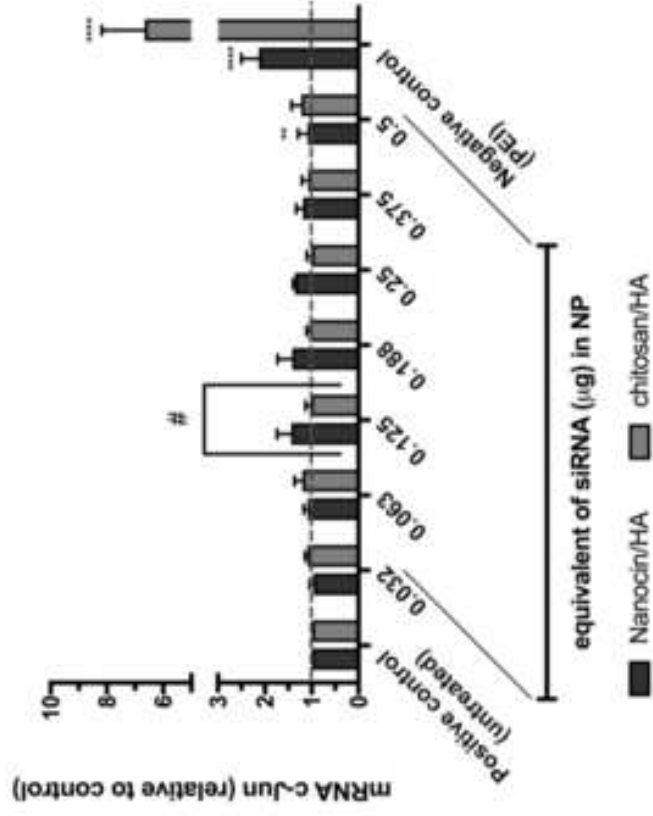


Figure S15



**a** | RT-qPCR: c-Jun expression



**b** | RT-qPCR: c-Fos expression

